



**LIVER VOLUME COMPUTATION FROM COMPUTED
TOMOGRAPHY (CT) IMAGES**

SARA OSAM SALIHI

FEBRUARY 2016

**LIVER VOLUME COMPUTATION FROM COMPUTED TOMOGRAPHY
(CT) IMAGES**

**A THESIS SUBMITTED TO
THE GRADUATE SCHOOL OF NATURAL AND APPLIED
SCIENCES OF
ÇANKAYA UNIVERSITY**

**BY
SARA OSAM SALIHI**

**IN PARTIAL FULFILLMENT OF THE REQUIREMENTS FOR THE
DEGREE OF
MASTER OF SCIENCE
IN
THE DEPARTMENT OF
MATHEMATICS AND COMPUTER SCIENCE**

FEBRUARY 2016

Title of the Thesis: **Liver Volume Computation From Computed Tomography (CT) Images.**

Submitted by **Sara Osam SALIHI**

Approval of the Graduate School of Natural and Applied Sciences, Çankaya University.



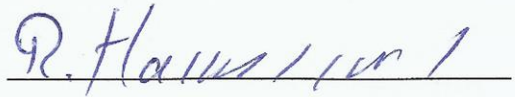
Prof. Dr. Halil Tanyer EYYUBOGLU
Director

I certify that this thesis satisfies all the requirements as a thesis for the degree of Master of Science.



Prof. Dr. Billur KAYMAKÇALAN
Head of Department

This is to certify that we have read this thesis and that in our opinion it is fully adequate, in scope and quality, as a thesis for the degree of Master of Science.



Assist. Prof. Dr. REZA HASSANPOUR
Supervisor

Examination Date: 04.02.2016

Examining Committee Members

Assist. Prof. Dr. REZA HASSANPOUR (Çankaya Univ.)



Assist. Prof. Dr. ABDUL KADIR GORUR (Çankaya Univ.)



Dr. BARIS TASBAS (Memorial Has.)



STATEMENT OF NON-PLAGIARISM PAGE

I hereby declare that all information in this document has been obtained and presented in accordance with academic rules and ethical conduct. I also declare that, as required by these rules and conduct, I have fully cited and referenced all material and results that are not original to this work.

Name, Last Name : Sara Osam SALIHI

Signature :



Date :

04.02.2016

ABSTRACT

LIVER VOLUME COMPUTATION FROM COMPUTED TOMOGRAPHY (CT) IMAGES

Sara Osam SALIHI

M.Sc., Department of MATHEMATICS AND COMPUTER SCIENCE

Supervisor: Assist. Prof. Dr. REZA HASSANPOUR

February 2016, 105 pages

Recently, the computed tomography images have been used explicitly for diagnosing of liver disease, as well as, they are used to measure the volume of the treatment and relocate of liver. In general, the liver is segmented by the medical images using manual or the computed tomography segmenting techniques because the characteristics surface of the liver and the effects of the partial volume makes the automatic discernment of liver from the other nearby organs very complicated process. Consequently, in this thesis we will suggest a semi-automatic technique for the liver for the purpose of measuring the size of the liver by using the tomography computed images. Thus, in order to segment the area of interest, we have to focus on the process of segmenting the liver based on the edge in addition to the techniques of the growing area. Finally, the investigational measurements of the size and area of the liver are consistent with those use for manual tracking methods for radiographic doctor and it shows that this algorithm is an effective algorithm to measure the size and semi-automated segmentation of the liver.

Keywords: CT liver, image segmentation, volume measurement, Region growing, Edge based.

ÖZ

BİLGİSAYARLI TOMOGRAFİ (BT) GÖRÜNTÜLERDE KARACİĞER HACİM HESAPLAMA

Sara Osam SALIHI

Yüksek Lisans, Matematik-Bilgisayar Anabilim Dalı

Tez Yöneticisi: Yrd. Doç. Dr. REZA HASSANPOUR

Subat 2016, 105 sayfa

Son zamanlarda, bilgisayarlı tomografi görüntüleri karaciğer hastalığı teşhis yanı sıra, onlar tedavi hacmini ölçmek ve karaciğer taşınmaya kullanılır için açıkça kullanılmıştır. Karaciğer ve kısmi hacim etkilerinin özellikleri yüzey yakındaki diğer organlardan karaciğerin otomatik muhakeme çok karmaşık bir işlem yapar, çünkü genel olarak, karaciğer kılavuzuna veya teknikleri segmentlere bilgisayarlı tomografi kullanılarak medikal görüntülerin göre segmentlere ayrılır. Sonuç olarak, bu tezde biz bilgisayarlı tomografi görüntüleri ile karaciğer boyutunu ölçmek amacıyla karaciğer için bir yarı-otomatik tekniği önerecektir. Böylece, faiz sipariş segmentine alanında, biz büyüyen bölgenin tekniklere ek olarak kenar dayalı karaciğer segmentlere sürecine odaklanmak zorunda. Son olarak, karaciğer boyutu ve alan araştırma ölçümleri radyografik doktor için manuel izleme yöntemleri için bu kullanımı ile ilgili olan ve bu algoritma boyutu ve karaciğer yarı otomatik bölümlenme ölçmek için etkili bir algoritma olduğunu göstermektedir.

Anahtar Kelimeler: BT karaciğer, görüntü bölümlenme, hacim ölçümü, Bölge büyüyen tabanlı Kenar

ACKNOWLEDGEMENTS

I would like to express my appreciation to my great supervisor, Assist. Prof. Dr. REZA HASSANPOUR, who provided me with unlimited support and valuable guidance. There aren't enough words to express thanks to you. I would like to thank BARIS TASBAS his assistance with the medical part. In addition, I would like to express my deep gratitude to my family: my dear father and my dear mother, and finally my sisters, brother and all of my friends for their endless and continuous encouragement and support throughout the years.

TABLE OF CONTENTS

STATEMENT OF NON PLAGIARISM.....	iii
ABSTRACT.....	iv
ÖZ.....	v
ACKNOWLEDGEMENTS.....	vi
TABLE OF CONTENTS.....	vii
LIST OF FIGURES.....	x
LIST OF TABLES.....	xi
LIST OF ABBREVIATIONS.....	xii

CHAPTERS:

1. INTRODUCTION.....	1
1.1. Background.....	1
1.2. Motivation.....	4
1.3. Thesis Challenges.....	5
1.4. Thesis Outlines.....	6
2. MEDICAL AND TECHNICAL BACKGROUND.....	7
2.1. Medical images	7
2.1.1. Ultrasound (Sonography).....	7
2.1.2. Digital mammography (DM).....	8
2.1.3. MR Imaging.....	9
2.1.4. CT Imaging.....	10
2.2. Medical Image Segmentation Definition.....	11
2.3. Abdominal Imaging.....	12
2.4. Anatomy of the Human Abdomen.....	12
2.4.1. Liver.....	13
2.4.2. Kidneys.....	14
2.4.3. Stomach.....	14
2.4.4. Spleen.....	14

3.	LITERATURE REVIEW.....	15
3.1.	Background	15
3.2.	CT.....	16
3.3.	MRI	16
3.4.	Liver Segmentation Method.....	17
3.5.	Subdivision of the liver segmentation methods.....	19
3.5.1.	Semi-automatic liver segmentation methods.....	19
3.5.1.1.	Graph methods based on semi-automatic.....	20
3.5.1.2.	Semi-automatic region based method.....	21
3.5.1.3.	The groups based semi-automatic method.....	22
3.5.1.4.	Semi-automatic method of matching ATLAS.....	23
3.5.2.	Fully automated liver segmentation method.....	24
3.5.2.1.	Automatic method based on deformation model.....	24
3.5.2.2.	Statistical Model C control method.....	25
3.5.2.3.	Atlas in the way of possible mechanisms.....	26
3.5.2.4.	Automatic methods based on cultivation.....	27
3.5.2.5.	Qaeda based on automatic.....	27
3.5.2.6.	Automatic method based on gray level.....	28
3.5.2.7.	Level Sets.....	29
3.5.2.8.	Edge Based.....	30
4.	PROPOSED SYSTEM.....	32
4.1.	Introduction.....	32
4.2.	Proposed System.....	32
4.2.1.	Image Enhancement.....	34
4.2.1.1.	Thresholding.....	34

4.2.1.2.	Histogram Modeling by using Adaptive histogram equalization (AHE).....	35
4.2.2.	Segmentation.....	36
4.2.2.1.	Edge Detection by sobel operation.....	36
4.2.2.2.	Segmentation based on regions.....	38
4.2.2.2.1	Definition of Region Growing.....	39
4.2.2.2.2	Basic Region Growing Approach.....	39
4.2.2.2.3	Geometric Characteristics of Regions.....	41
4.2.2.2.4	Basic concept of seed points.....	41
4.2.2.3.	Integrating Region Growing and Edge Detection.....	42
4.2.3.	Morphological algorithms (Hole filling).....	44
4.2.4.	Calculation of Liver Volume.....	45
5.	EXPERIMENTAL RESULT.....	46
5.1.	Overview	46
5.2.	Data Set	46
5.3.	Experiments	46
5.4.	Accuracy.....	69
6.	CONCLUSION AND FUTURE WORK.....	81
6.1.	Conclusion.....	81
6.2.	Future Work.....	81
	REFERENCES.....	R1
	APPENDICES.....	A1
A.	CURRICULUM VITAE	A1

LIST OF FIGURES

FIGURES

Figure 1	Liver image segmented.....	2
Figure 2	Similarities liver organ (A) similarity between the gray levels in the liver and stomach, (B) liver and heart.....	3
Figure 3	Ultrasound (Sonography).....	8
Figure 4	Digital mammography (DM).....	8
Figure 5	Magnetic resonance imaging (MRI).....	9
Figure 6	The Modern clinical CT scanner	10
Figure 7	Liver Segmentation Methods	19
Figure 8	Semi-automatic Methods.....	20
Figure 9	Flowchart Diagram of The System.....	33
Figure 10	(A)Image of CT scans before enhancement, (B) Result Image of CT scans after Applying (AHE).....	35
Figure 11	Sub steps of Segmentation Process.....	36
Figure 12	Sobel Edge Operators.....	37
Figure 13	After Applying Sobel Edge Detection.....	38
Figure 14	Start of growing a region.....	40
Figure 15	Growing process after few iteration.....	40
Figure 16	Frame 80 after segmentation.....	42
Figure 17	Selecting of the extra part of segmented place.....	43
Figure 18	After selected the extra part.....	43

Figure 19	(A) Image before applying Morphology, (B) Image after applying Morphology.....	44
Figure 20	A CT image series (a sequence of slices).....	45
Figure 21	(A) Frame 55 Original Image, (B) Frame 55 After Enhancement.....	47
Figure 22	(A) Frame 55 After Edge Based, (B) Frame 55 After Region Growing.	48
Figure 23	(A) Frame 55 Segmented Image, (B) Frame 55 After Morphological Operation.....	49
Figure 24	(A) Frame 100 Original Image, (B) Frame 100 After Enhancement.....	50
Figure 25	(A) Frame 100 After Edge Based, (B) Frame 100 After Region Growing.....	51
Figure 26	(A) Frame 100 Segmented Image, (B) Frame 100After Morphological Operation.....	52
Figure 27	(A) Frame 83 Original Image, (B) Frame 83 After Enhancement.....	53
Figure 28	(A) Frame 83 After Edge Based, (B) Frame 83 After Region Growing...	54
Figure 29	(A) Frame 83 Segmented Image, (B)Frame 83 After Morphological Operation.....	55
Figure 30	(A) Frame 56 Before Using Manually Operation, (B) Frame 56 After Using Manually Operation.....	56
Figure 31	Frame 56 Segmented Image.....	56
Figure 32	Different Shapes of Liver, (A) Frame (50), (B) Frame (52), (C) Frame (66), (D) Frame(81), (E) Frame (101), (F) Frame (200), (G) Frame (295).....	56
Figure 33	Confusion matrix.....	69

LIST OF TABLES

TABLES

Table 1	The result of simulation from frame 50 to 324.....	59
Table 2	Assessment the accuracy and specificity and sensitivity from frame 50 to 324.....	70

LIST OF ABBREVIATIONS

CT	Computed Tomography
LSM	Level Set Method
JPEG	Joint Photographic Experts Group
BMP	Bit MaP
MRI	Magnetic Resonance Imaging
USG	Ultrasonography
PET	Positron Emission Tomography
SPECT	Single-Photon Emission Computed Tomography
ROI	Region Of Interest
DM	Digital Mammography
1D	One Dimensional
2-D	Two Dimensional
3-D	Three Dimensional
IVC	Inferior Vena Cava
HCC	Hepatocellular Carcinoma
AHE	Adaptive Histogram Equalization
HE	Histogram Equalization
TP	True Positive
TN	True Negative

FP	False Positive
FN	False Negative
CADx	Computer Aided Diagnosis
DICOM	Digital Imaging and Communications in Medicine
SBRG	Seed-based region growing
MI	Mutual Information
EM	Expectation-Maximization
KNN	K nearest neighbor

CHAPTER 1

INTRODUCTION

1.1 Background

In modern hospitals there are a large and growing tendency to use software explanations and the computers to assist the doctors in the process of diagnosing, analyzing and handling of many diseases. The assistance that received by the doctors from the computer hardware and programs often be a digital photos taken from different parts of the human body. Furthermore, through these images the doctors can watch the internal organs of the human body without the need for an effort and the images consist of different numerical methods such as Magnetic Resonance Images, CT scans as well as X-rays. These modern scanning and imaging technologies are considered great development of operations on traditional and analogue techniques that were used previously. Examples of modern digital hybrid imaging technology are digital X-rays, which can be analyzed easily by using the computer because it is with digital format. As well as, the X-rays are considered less noise compared to the analogue techniques that used in the past. Besides, resonance magnetic and Computed tomography imaging provide very accurate visions to the human body which were not presented in the techniques that were used in the past. So, doctors have the ability to can get an accurate information about the disease suffered by patients through multiple imaging technology that is used in clinical operations. Moreover, the development of computer and medical imaging technology created chances to take medical image and measurable analyzes of the human body. They provide powerful techniques to study pathology and function. The availability of accurate and quick results in all aspects of image processing of many different imaging modalities has increased the need to achieve another significant improvement.

Current research areas that interest for diagnosis by using the imaging are interested in diagnosing members of abdominal from which are liver, kidney, gallbladder and spleen. Diagnosis includes the study of anatomical structures and the measurement of the volume of tissue, treatment planning, segmentation, pathology and computer-assisted surgery in the localization, is an important step for radiological procedures. The manual segmentation process, due to the high number of slices, is boring. Not only is it time consuming, it also depends on the operator's skill and experience. For example, Figure 1 shows a liver sample image segmented in a Computed Tomography (CT) Image.



Figure 1 Liver Image Segmented.

Many are given different segmentation techniques and developments in this area [1] have been increasing every year. However, currently it provides successful results for all types of medical images and even different imaging modalities have no segmentation technique for the same organ. For example, liver and brain segmentation conditions differ.

In other hand, the requirements of the dividing liver by using Magnetic Resonance Imaging in addition to Computed Tomography, all of them conducted by a different segmentation, so, the segmentation of organs through medical images continued to be an unsettled issue. Additional cause which beam hardening, construction works and noise caused by the movement of patient image works as a quality deterioration is that it causes blurred boundary. Lead changing conditions. In addition, liver, kidney and heart in different positions with are adjacent organs and has a very similar density value. Liver ultrasound imaging can be performed with CT and MRI. When compared to MRI images, CT images have a higher contrast resolution. Such good soft tissue contrasts of MR indicates that there are many advantages such as the free form of ionizing radiation for image navigation and multi-planar capabilities. However, it is more difficult in the Mar automatic segmentation of CT images. Because small edge magnitude causes edge-based segmentation, the algorithm is more complex than the CT images. Moreover, depending on the MRI pulse movement, it leads to partial volume effects and works more automated liver segmentation challenge. Therefore, [2] compared to CT based liver segmentation approach. There are few studies in the literature for liver MRI image segmentation [3], [4], [5], [6]. Data sets example with abdominal MRI, gray level because of similarities to show cause liver segmentation is hard work are shown in Figure 2.

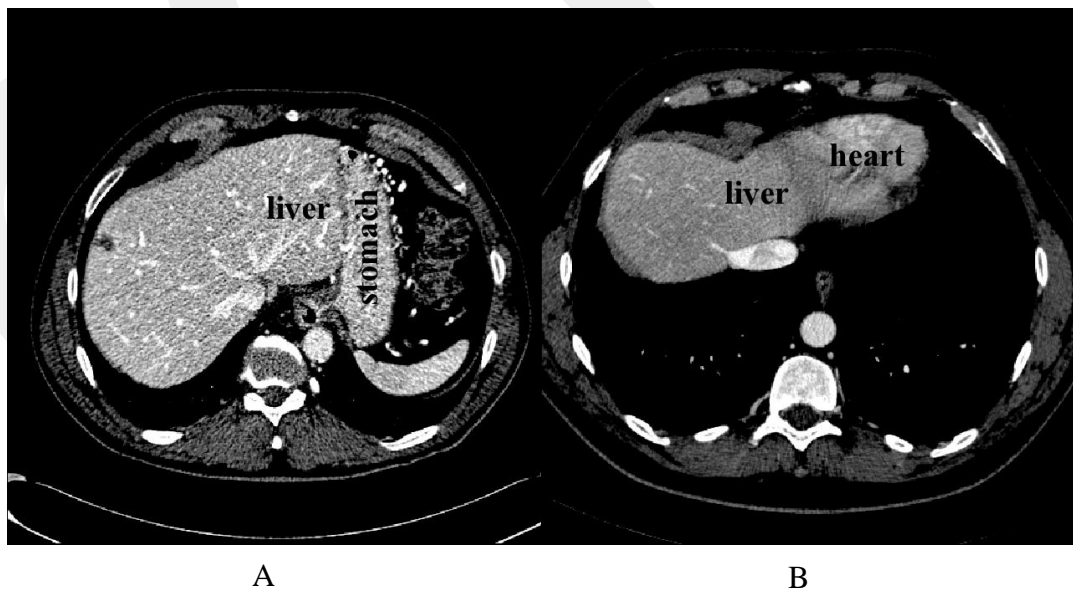


Figure 2 Similarities in the liver organs (A) Similarity between the gray levels in the liver and stomach (B) liver and heart.

1.2 Motivation

For the purpose of imaging the inner configuration of the human body we apply the methods of medical imaging on a large scale in the field of Diagnostic Radiology which take different types including Computed Tomography (CT) [7], Magnetic Resonance Imaging (MRI) [8], Ultrasonography (USG) [9], [10], Positron Emission Tomography (PET) [11] and Single-Photon Emission Computed Tomography (SPECT) [12]. For assessing liver disease, we often use CT, USG and to a few extent we use MRI. In this study, we will emphasis on the exploration of the CT images that belong to the liver. According to the change in the amount of X-rays gripping the human body the CT images being produced. In the surgical operations that applied to the liver surgery, the extremely variable hepatic vascular construction confuses the planning and the execution of the surgical procedures [13]. The process of the anatomy of tumor or lesions in the liver causes in cutting the blood supply to other parts of the liver and thus being loss and sacrifice proper cells in the liver. According to various hepatic vessels that feed all parts of the liver, the liver is divided into eight parts or functional sectors [14]. In the medical operations that take place in the liver for the purpose of eliminating the pathological region, those operations should be balanced and do not affect adjacent healthy parts of the liver for the purpose of preservation of those parts. Liver size is determined piece by piece through the use of CT images and physical representation of sliced or neighboring pieces. In order to determine ROIs that belongs to the liver specifically, it necessitates the precise analysis of medical images that are taken from the liver in different ways (as mentioned previously) by specialist doctors. The border among the purposeful blocks or slides of the liver to be identified by a large group of hepatic veins and veins portal [14] [15]. However, the borders of the liver frequently do not draw in good and accurate forms. Overall, the process of division or fragmentation of the image obtained from the liver passed through several operations, a pre-treatment process and the major segmentation process and finally, the post-treatment process. Pre-treatment process on which to arranges and regulates the image data that have been taken in order to fitting the main retail operation. The operation of post-processing work to improve and mending the

cutting of the results of a preliminary process in order to give ROI of the most likely area that was used. To increase efficiency, the pre-processing of liver segmentation will include the threshold level for images to be able to remove the pixels from isolated places such as air, bones as well as, body liquids. Materials which symbolized by CT images in which the high-density areas are located away from them being simply removed by clarifying with some stable threshold values.

Later, the image being moderate and the noise will be removed by the CT images after the X-ray scanned parts of the body. Before the preliminary data of the image being processed using computer algorithms, the image should be adjusted for several times, whereas, the re-adjustment is premeditated by the parameters that derives from the header of the image. A major retail operation to regulate the process of identifying edge and extracting the ROI from images of the CT. The most challenging problems that draw the segmenting algorithms is the discrepancy in the liver shape and its non-clear-cut boundaries, because the liver is on the edge of tissues and other organs. Up-to-date methods using a range of different technologies in order to address such issues in automatic or semi-automatic approaches and these approaches include thresholding, region growing [14], [17], level set segmentation [18], probabilistic modeling and statistical [14], active contouring (GVF) [19], clustering, template-matching, voxel classification, adaptive histogram equalization, [20], graph-cuts [21] and neural networks [22].

1.3 Thesis Challenges

The process of segmenting the liver in the images of CT is not an easy matter as it is a complicated work due to the following influential factors:

1. Abdomen images that are taken by the CT images might be on a gray format instead of color.
2. The liver will take different sizes and shapes from patient to patient.
3. The similarity to other organs making it harder to identify clearly the liver from other organs.

4. The difficult to differentiate the liver from the other organs because of it resembles to the other organs.
5. The difficulty of the anatomy of the liver.
6. The nature of liver tissues.

1.4 Thesis Outlines

The chapter of this research has been arranged as follows:

Chapter One- Introduction: This chapter shows the motivations of the thesis project, challenging and thesis outline.

Chapter two- Background: This chapter shows the medical images, Abdominal Imaging, Anatomy of the Human Abdomen

Chapter Three- Literature Survey: In this chapter a survey of previous studies in image processing.

Chapter Four- Applied Methods And Proposed System.

Chapter Five- Experiments and Results.

Chapter Six- Conclusions and Future Work.

CHAPTER 2

MEDICAL AND TECHNICAL BACKGROUND

This chapter has been separated into four parts, the first part will deliver a medical images, the second Abdominal Imaging, the third Medical Image Segmentation Definition followed by Anatomy of the Human Abdomen.

2.1 Medical Images

Since the discovery of Aloha (X-ray) rays by German physicist Wilhelm Roentgen 110 years ago, and more specifically in 1895, radiology has been evolving rapidly. The detection of radiation since the beginning of the last century has had a great impact in various fields of medical diagnosis and it has evolved to use radiation therapeutically [23] [24]. There are diagnostic radiology devices which do not use X-rays, including ultrasound imaging and MRI Magnetic Resonance Imaging (MRI).

Different types of Diagnostic Radiology include:

- 1- Ultrasound.
- 2- Computed Tomography (CT) scan.
- 3- magnetic resonance imaging (MRI).
- 4- Mammography devices.

2.1.1 Ultrasound (Sonography)

That process of exposing an area of the human body to high-frequency sound waves to guise the human body and create an image of the organs that inside the human body is called ultrasound imaging. The frequency of ultrasound begins with 20 kHz.

Ultrasound does not look like X-rays because the visible scan is not used in ultrasound, which used in X-ray because it (ultrasound) is captured in real time and can display the structure of organs in the human body. As well as, through ultrasound we can watch the movement of blood flow in blood vessels, in addition, to watch the movement of the organs in the human body. Using ultrasound, doctors can diagnose and treat many medical cases, also, ultrasound is considered as portable by MR and CT, as well as, it is considered relatively cheap.



Figure 3 Ultrasound (Sonography)

2.1.2 Digital Mammography (DM)

One of the latest techniques in the medical imaging field is mammography, which has become high contrast, working with high resolution film, thereby making it very suitable and useful to examine the breast. In fact, this technique basically is an X-ray, which uses a low-energy X-ray system usually around 30 kvp (an X-ray technique that is still used frequently in medical imaging and is considered to be the oldest technique).



Figure 4 Digital mammography (DM)

2.1.3 MR Imaging

MR imaging is used dramatically through multiple clinical resolves, and will be used in the upcoming in more intensively. Clarification of images that been taken by MR will be depending on how the image was obtained. By understanding the basic principles of magnetic resonance imaging, we can improve the quality of the image being taken by MRI.

Consequently, the images obtained by magnetic resonance be very understandable and very important. Nevertheless, according to the opinion of many radiologists and doctors, the images taken by MRI are difficult to obtain because it monitors through electromagnetic detection based on resonant frequency. Furthermore, when comparing images that are taken by MRI with other imaging techniques, the MRI provides degrees of freedom in obtaining information through it. The fundamental struggle that exists in various forms of magnetic resonance imaging is the result of its technique, which includes digital signal processing, physics, mathematics and electronics. In the literature, there are many articles on the moralities of MRI [25] [26] [27].



Figure 5 Magnetic Resonance Imaging (MRI)

2.1.4 CT Imaging

There are wide applications for the CT scanner, it is used in radiology as well as in many clinical situations and also, it's considered a relatively cheap technique. Imaging by CT scanners is also be used to measure the reduction of X-rays. The reduction of X-rays happens by circling the tube of the X-ray round the patient using sensors located on the framework [28]. The previous mathematical techniques and measurements are used to recreate 2-D data by consuming multiple 1-D projections thereby producing 2-D cross-sectional images. In addition, the advancement of medical technology have been added many ways to develop the imaging by CT. By recycling CT tube in one direction around the patient the CTs helical or spiral is getting. Through the continuous moving tube, the table where the patient is relocated through the beam of the X-ray. Also, this technique can offer the obtaining of information as incessant Furthermore, one of the main benefits of this method is to reduce the speed of acquiring, through which we get the data volume without registry errors that occur during patient movement [29]. In recent years CT scanner become use the similar concept which is used in spiral scanners. Moreover, CT scanner has multiple rows as well as detection rings through which they can acquire multi-slice in each session of the tube of X-ray [29].



Figure 6 The Modern clinical CT scanner

2.2 Medical Image Segmentation Definition

It is well known that the interpretation of medical images process is a very substantive process, so there is an increasing need to highlight the process of image processing in order to facilitate the work of radiologists in the diagnosis of diseases.

Moreover, Image segmentation process is considered as the first step of the most important responsibilities in the analysis image processing operation because the segmentation results affect every successive process of image analysis processes, including the description and representation of the element and measuring feature and even the supreme importance of the tasks, including the classification of the object. So, the importance of the segmentation of image is of the main tasks in order to facilitate the categorization process of the interesting areas. The image segmentation by manual process is considered inaccurate, especially with the growing and evolving of medical imaging methods over time, also, it is a tedious process and time consuming. Experiences by experts have shown that the ways of manually segmenting of resulting in a change in the shape of the image by 20%, for that it is preferred to use the mechanism of algorithms which are accurate and take less time of interacting with the user. When doing the segmentation operation on the image the region of interest in the image must be extracted and seen only. So, we can define the image segmentation process as the segmentation of digital image to several regions in each regional group of pixels. The main purpose of the segmentation process is to restrict and shorten the image to make it clearer and simpler in the process of analysis. The results of the image segmentation process is to get a set of parameters that are extracted from the image or extract a group of regions that combined covering the image [30]. Finally, according to the combined of reasons mentioned above, it is more accurate to define the segmentation of medical image process, as the separation process and the demarcation of the area of interest so that it can be displayed individually in order to obtain an important tasks, such as the patient's diagnosis, planning process and research treatment for more relevant and accurate operations.

2.3 Abdominal Imaging

One of the important disciplines in Diagnostic Radiology is an abdominal imaging process that delivers diagnostic imaging and the participation of disorders of the abdomen and pelvic. The specialty of Diagnostic Radiology offers an extensive clinical trial for the care of patients and the interaction with the surgical and medical specialties. Digital images processing technology are used in order to citation further exhaustive information for small dimensions of surgical and therapeutic methods using different imaging processing techniques. Moreover, there are many different medical imaging modalities for human abdomen, also, there are different parts of the body being used to get the data [31]. Also, there are different ways to rebuild the image as the CT images and X-rays which are used to get information roughly the mass of the tissues. Moderation and excitation tools of the thickness of the proton been in use such as MR imaging. MR Spectroscopy (MRS) imaging depends on the substances of the tissues. Many kinds of tracers are added through a vessel prior to the acquisition in Single Photon Emitted Computed Tomography (SPECT) imaging and Positron Emission Tomography (PET). Likewise, we can obtain different information by using the same type of imaging technique over dissimilar ways for instance different tracers in SPECT and PET, the injection of contrast agents in MR or CT and dynamic acquisitions.

2.4 Anatomy of the Human Abdomen

The abdomen is considered the important part of the human body and be almost on cylindrical chamber constitutes the most important part of the body and located between the superior margin of the pelvis at the pelvic brim and the inferior margin of the thorax at the thoracic diaphragm. The bottom hole in the chest is the top slot for abdomen of the human which is locked by the diaphragm, whereas, the abdominal wall it is the limits of the abdominal cavity. The human abdominal wall is muscle structure that is protected by fascia, skin and fat which is continuous with the pelvic wall at the entrance to the pelvis. Abdominal viscera are the key elements of the digestive and skeletal large nerve vascular and urinary tract, kidney and abdominal viscera be located between the cavity wall and musculoskeletal or be suspended in the cavity

protease by mesentery [32]. The abdomen is considered one of the important functional parts in the body, it contains the digestive system, which works to assist in the digestion of food and nutrients that have been absorbed process. Digestive system located in the abdomen consists of the esophagus, jejunum, duodenum, stomach, appendix, cecum, sigmoid colon, ileum, transverse, the rectum and ascending and descending colons. There are other organs to be directly connected with the process of digestion, including the liver, kidneys, pancreas and spleen. All organs, which are found inside the abdomen be a pipe shape. In addition, the digestive system contains a number of interconnected and related organs, including stomach, colon and small intestine and appendicitis. However, liver, pancreas, gall bladder be related to the digestive system. Other tissues that belong to the digestive system, a kidney, spleen and lymph Physiopathology be linked with each other through the blood vessels, including the inferior vena cava and the aorta. There is a flexible membrane protein covering the pelvic organs which is the urinary bladder, uterus, Fallopian tubes and ovaries also covering most of the human organs.

2.4.1 Liver

The liver is one of the biggest organs of the body and its color is reddish-brown and located in the right upper quadrant of the abdomen human, it weighs is about 2% or 3% of the whole weight of the body [33]. The liver does not take a particular shape in a certain way where its shape according to the adjacent structures for instance the diaphragm and lower ribs. The liver may be small in size and is located at the right part of the abdomen or spreads to the left and shielded by the spleen. The largest vessels in the liver are the portal vein and hepatic veins, and the liver has lobes, which are associated with blood vessels. The most important functions of the portal vein that existing in the liver is to bring blood from the intestines and spleen and pancreas. The inferior vena cava drains the three hepatic veins. There are many structures that explain liver autopsy one of the most prominent and widespread is the new autopsy, which divides the liver and is presented in [34]. Couinaud suggested the most common way in which to view the comprehensive overview of the liver [35]. Liver contains eight cloves covered by the portal vein. One of the most important functions of the liver is to regulate biochemical reactions, including the construct or collapse small or the

complicated molecules. Furthermore, the liver also produces bile, which is a composite alkaline digest which emulsifying lipids.

2.4.2 Kidneys

There are two kidneys in the human body are located on the right and left side of the spine, the left kidney is located below the diaphragm behind the spleen, while, the right kidney location below the diaphragm behind the liver. Kidneys are significant members of the human body is important for homeostatic functions, for instance the acid-base balance and the absorption of amino acids and glucose, blood pressure, in addition to its importance for the digestive system. Moreover, the other kidney functions are carrying the blood from the opposite renal arteries to the paired renal veins.

2.4.3 Stomach

The stomach is a flexible muscle organ located in the upper left area of the abdomen which takes the form of a pear. The stomach is considered expandable organ that works on moving the food violently after the munching stage. The shape and size of the stomach, usually adjustment subject to the quantity of food within and it is typically accommodated on one liter of food. When food enters the stomach from the esophagus, the stomach using infectious squeezers in order to digest food. The wall of the stomach is almost similar to other organs of the digestive system in spite of the presence of an additional related layer into the circular layer.

2.4.4 Spleen

A spleen weight is about 150 grams and its length is about 11 cm in the adult and healthy people. Furthermore, the spleen is usually located in the left upper quadrant of the abdomen. The functions of the spleen are fighting the infections and germs that enter the body, as well as, it filters the blood from some exotic material, also, it analyzes the old cells and production of lymphocytes, in addition, it stores the blood.

CHAPTER 3

LITERATURE REVIEW

3.1 Background

The liver is considered the directly in charge of the creation process of biochemical substances necessary for digestion, detoxification and creating a protein.

The liver is the vital organ that's been in the human body and locates in the right higher part of the abdomen and is responsible for many important functions in the body. Liver infection can be one of the main causes of increased mortality in the world with hepatocellular carcinoma (HCC) being one of greatest dangerous illnesses that damages the liver [36], [37]. Recently, many diseases have been diagnosed with by computer science that had a great importance in this area, especially liver diseases, for example HCV, HBV, liver fibrosis, cirrhosis and HCC. Computer technology has been provided powerful techniques called image processing techniques can use in the assessment and diagnosis of liver diseases. In recent years, the area of medical image processing has been developed and become an important field which many techniques including the segmentation of the liver using CT image have been used.

This is the main important step that is necessary for the liver disease diagnosing; it measures the size of the liver. The anatomical information extracted from liver large amounts of data requires a visual inspection process is manual and time-consuming process is hacked great mental work. The concept of image processing machine learning methods and in many styles and semi-automatic filling of divisions the liver. However, the segmentation of liver CT images is a challenging mission according to the low level of diversity edges that illustrate the image of type CT. Because of these properties as a minor effect because of the patient, on average, Space movement, antiques restoration and beam hardening. Furthermore, the surrounding organs, for instance the stomach, spleen and liver, may be sharing the same gray levels. At the

same time, the gray levels of similar devices may not appear in the similar issue. Which increases the difficulty of the mission in addition to the previous finding is the complication and the presence of a wide range of retail formats. In general, the way to divide the liver using CT images into two main categories, and divided the liver automatic methods and semi-automatic methods. Most of these methods are explained/expounded upon in the following sections.

One of the important stages of liver segmentation in computer aided techniques for the analysis of liver disease. Investigators have provided numerous methods for segmenting the liver. However, segmentation of the liver is a complex and challenging process for two reasons. First, there is the intensity (overlap) between the liver and nearby tissues, for example the kidney and the heart. In addition, the division challenges due to the nature of the shape of the liver that take the form of non-rigid [38], [39].

3.2 CT

Many different techniques of automatic and semi-automatic segmentation are available for the liver using CT data sets run in the literature [38]. We can divide this group of liver CT images using a neural network (Tsai 1994) [40], based on morphological operations Bae et al. (1993) [5] and deformable models. However, problems originating from the liver's geometrically complex data sets with low contrast and different characteristics of adjacent tissue together in this method are used.

3.3 MRI

According to our knowledge, there is no study for the purpose of a review of the segmentation method of liver by using magnetic resonance. Moreover, through our study, we noticed that there are few studies of magnetic resonance imaging, which work on the liver segmentation and one of these studies was to Nowozin and Lixu (2005) [41], is three phase, where a seed area uses a quick march and initializes a division that is based on the applied level. The first approximation of the liver uses the

quick march. This form is used for the initial stage. The segmentation results have been better. However, the conclusion may be further research on the study of the performance of the algorithm of segmented objects of different and unusual shapes. Another way to classify liver MRIs in Hermoye et al. (2005) [42] is to regulate the size of the liver in living transplant donors. The physical size of the liver connected with weight and expected in this study the liver to have a density of units using the level of the group. As recognized by the authors, range (Delineation) and reform of the liver after the manual segmentation method is required.

The MRI 3D liver segmentation method based on network sync oscillators Strzelecki et al. (2007) [43] is additional method. The oscillator network has been defined by a differential equation. Oscillators have been associated with a three-dimensional network shape and the network size image has been evaluated wherein represents a pixel oscillator. Each oscillator with global inhibitors which receives information from the oscillators and the network can be connected to the harness. Because of the local excitatory connections, an oscillator extends its activities to the oscillator that represents the object image.

3.4 Liver Segmentation Method

It is sometimes difficult to persuade doctors to carry out automatic segmentation. They usually adopt manual methods. For this reason, we focus on finding a liver segmentation method that automatically yields accurate results compared with guidelines introduced by experts.

We describe a useful and accurate technique for segmentation of the liver, which was conducted in three main phases. Every CT image from the liver Imaging Atlas (online reference for imaging the liver) was collected. The collected images were in 512×512 JPG format, where each image represents a patient. The data were collected in two sets: 13 photos and 56 normal CT infected with CT images. Every image has been altered to gray scale format and saved in a 256×256 format. This became the most used technique.

After selecting the appropriate data collection, the segmentation process with primary liver CT images is extracted by analyzing the histogram of the gray images [44]. This

process of experience histogram of gray images is ready to find the potential severity of the liver is called the threshold, the process of searching for a range of values in which pixels liver. Histogram range of 69 gray images which test for the liver.

The liver is the largest internal organ in the human body. It performs a diversity of life sustaining functions and affects every physiological process in the body. It acts as a blood purifier, nutrient processing unit and it also controls the metabolism in the body. It primarily controls red blood cell decomposition, plasma protein synthesis and hormone production. Computerized tomography processes a series of X-ray views taken from different angles to create cross-sectional images of the bones and soft tissues inside the body. A CT scan of the liver is used to assess the liver and its related structures for various abnormalities when other types of examinations are not conclusive. It is also used for cancer detection and to provide guidance for biopsies. Image segmentation plays an important role in medical image analysis. An accurate segmentation of the liver is crucial in clinical diagnosis and study. Pre-processing of liver CT images is required for accurate liver segmentation. The extraction of the liver's anatomical information from the abdominal CT image requires a great amount of expertise and it is time consuming [45].

Several algorithms have already been implemented to segment the liver from abdominal CT images. Shraddha Sangewar et al. [46] performed liver segmentation using the modified K-means method along with a specialized contouring algorithm. Suhuai Luo et al. [47] proposed a liver segmentation technique using wavelets and machine learning. Hans Burckhardt et al. [48] applied a hybrid segmentation algorithm to perform liver segmentation. Other methods include the adaptive fast marching method [49], local entropy based method [50], region scalable fitting model [51], a pseudo colorization approach [52], statistical model [53] and graph partitioning approaches [54]. However, great challenges still remain in liver extraction in terms of accuracy, automation and robustness.

3.5 Subdivision of the Liver Segmentation Methods

In general methods of dividing the liver using CT images divided into two classes automatic and semi-automatic liver segmentation mechanisms. The following sections include giving further details on these mechanisms.

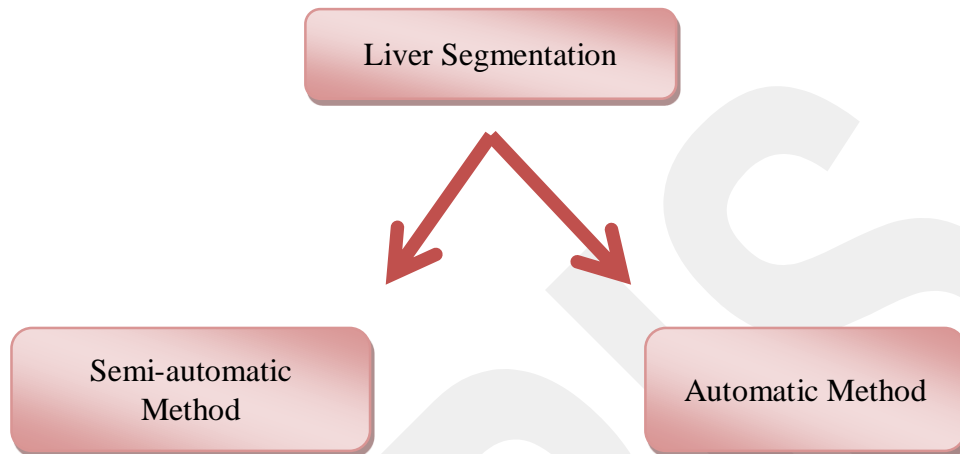


Figure 7 Liver Segmentation Methods

3.5.1 Semi-automatic liver segmentation methods

The process of liver segmentation using semi-automatic manner includes an imperfect user interpolation in order to complete the mission.

Interpolation may differ from the selection by manually of seed pixels to a manually refinement of a binary mask to the liver. After that, methods include semi-automated process to divide the liver were displayed in different ways according to the images processing techniques that been used. Half-way to complete the work of the liver requires limited user intervention. The intervention from manual collection of correct user manual for seed pixel binary mask to the liver. Then, the semi-finals of the fragmentation of the liver are presented according to the technique of images used, treatment is prearranged.

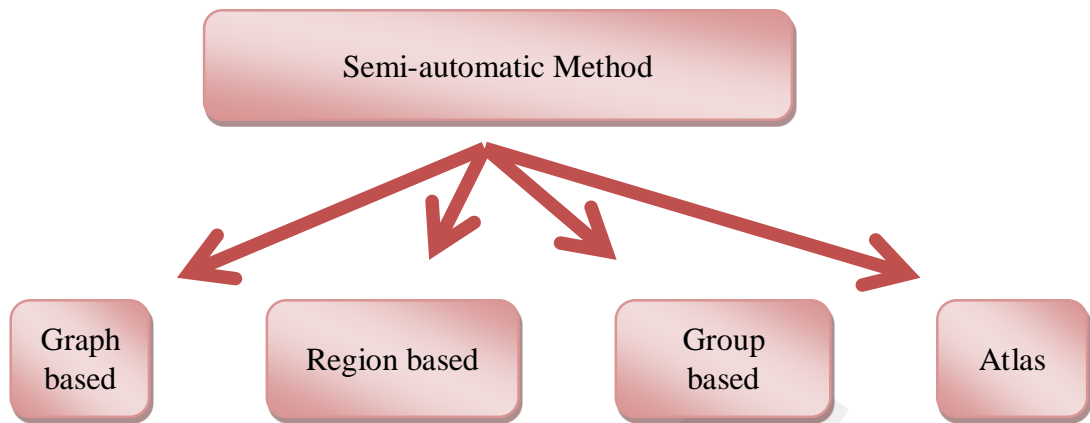


Figure 8 Semi-automatic Methods

3.5.1.1 Graph methods based on semi-automatic

This is followed by photos and diagrams weight and non-directed, where the pixels/ voxels showing peaks treatment, and neighboring pixels/ voxels are considered to be connected vertices. Weight edges of the similarity measure between the two peaks are relevant. Works in seed selection and payment process user interaction diagram method. In general, live in this category algorithm and graph algorithms wire break apart.

At [7], they introduced wired segmentation algorithm for extracting the border from medical images. The invented algorithm computes the least cost routes through a set of points in the image they want to study its characteristics such as direction and gray. The amount of the slope and zero Laplace passwords are used to calculate the cost of a mass. The user specifies the initial seed point within the device, the dynamic programming algorithm a search algorithm has been utilized to calculate every possible lowest cost path, beginning from seed argument to remainder of the image with the border set by the user interaction device. In [8], they proposed a way to divide the live wire of the liver in the CT direction and reduce the interaction between the user and the computing time.

The live wire segmentation algorithm with a user control and segmentation process is complete. The mission with the seed selection and choice of users will be limited to requirements at the border, while the computer handles the details of the procedure. In [9], they proposed an algorithm for graphs in their research work. The liver 3-D segmentation approach, using interactive images is provided by the CT-based segmentation method for the cutting diagram [10] and refining stages. The initialize method is as follows: it is one sign (or more) of the liver areas classified by Member State. The grain background is automatically adjusted.

3.5.1.2 Semi-automatic region based method

Segmentation according to the region depends on grouping a number of pixels, or according to the region on consistency standard of the characteristics of that region. Furthermore, this consistency is usually depends on the density, texture, color, or it may depend on a composition of these factors. This segmentation method supposes that neighboring areas have dissimilar features. In addition, this method relies on two areas. The first is the technique of the merging basis which put seeds on the input image. Then, these areas which are close to the seeds regions are tested to see if they achieve the consistency standards. The selecting of these areas is done frequently result of growth in these regions until no more areas are that satisfy the standard conditions are found. In addition, if there are two regions that satisfy the same standard condition they will be combined into one region. Mancas et al., [55], is discovered one of the examples that has used this method, where he used the region's growing method in order to segment the objects in medical images that have the same standard unification. The authors included the spatial space from the point to the seed to the algorithm of growing area, which lead to the emergence of a map which collects the pixels according to the similar intensity of their seeds and also according to the space between the pixel and the seed. Furthermore, the experiment conducted by the author showed that the method of the growing region method can evaluate the object accurately from the medical images with noise. Pohle and Toennies, [56], have developed an algorithm that uses the growing region by segmenting the medical images, where this algorithm works on learning the homogeneity standards from the features of the target area.

However, according to use the unacceptable chose of the place of the seed, that's will results in decreasing the probability of poor performance. In addition, there is another technique that called as the region splitting, where the input image is defined in it as a single region, which will lead to segmenting of the region to smaller regions until there is no ability to segmenting the single region to more regions and that will result the segmenting image. The more development technique to developing the standard region is known as "merge and split". Moreover, one of the additional features in this region is that sometimes in the algorithm for evaluating the region as ordinary, over-splitting occurs in the segmentation process when we have two adjacent areas. The more developed methods are to merge these over-splitting regions. Liu and Sclaroff, [57] have used the split and merge algorithms to execute the splitting process. Also, Liu and Sclaroff, [57] have been routed typically (as will be explained later). In general, the techniques of based region are considered as a successful method when the regions inside the image achieves terms unification and follow the supposition. However, this method is used rarely in practice because the natural image usually has noisy and the borders between objects are not defined obviously. Moreover, the splitting depending on the region is always depends on many factors like the size of the seed as well as, the unification parameters of standards. The process of putting the seeds badly may lead to unsegment regions, as well as, the process of choosing some parameters to the unification parameters may lead to segmented regions and not be back to a single group or dingle region or it may get on single region been segmented by mistake. In [11], they are growing every area of the algorithm in their approach to segmentation of the interaction of the liver. The core of the proposed method is that the 3D field with standard connection areas just leaked or missed parts manually by using processing after being stretched and divided by the convex Account Body housing it in local areas around the limit.

3.5.1.3 The groups based semi-automatic method

This problem of image segmentation algorithm level group company by asking the user to draw a rough contour outside or inside the body, and then will Cantor/ small format. When meet contour object limits, to terminate the contract/ model is

developed. Performance a key role in controlling the direction of the contour of Shrine KAG / growing and find the end point plays practice. Segmented liver procedures under this category are divided into two sub-categories. Level 2D, 3D method of determining the level set method.

In [12] the liver is split on the basis of a 2-D set of dynamic performances that suggest speed. Thus, the raw contour manually in the number of CT in liver snow SL was created. She works the speed specified by the novel. [13] Consistent performance over any repeat captivity D is critical. The basic principle is that the system design and operation speed does not have to stop when a function of the speed is equal to zero on the border device. In turn, the contour path elephants system and uses this information to define performance. When Cantor isolated pixels that are likely to cross the border as part of the liver, it keeps the deployment process. If it exceeds a few pixels underpasses, the proliferation slows down significantly. This process will continue in this manner until it stops. Verge morphological and processes provided by [14] are working to extract the chest, reduce fat under the skin to the method of execution, and use the results of the extraction step as a function of speed blocks in the area. The method described [15] a level of 3D, which requires a moderate level of intervention is to divide the liver in CT slices. 2D user a number of signs in the form of re-sampling of the plane orientation (preferably perpendicular to each other.) Select the features defined by the points on the border of the liver, the interpolation using the cubic keys. After the user set 6-8 features, radial basis and works provided by work [58] for passing through all the characteristics of a flat surface and inside of them. With this level as a geodesic active contour configuration on the edge. As is usually the case in the vicinity of the border of the liver's right, no need to force a steady pace through the development of a surface. Using a set distance from the current level of the input parameters specified by the user an additional term to keep the shape.

3.5.1.4 Semi-automatic method of matching ATLAS

Chance of manual segmentation Atlas of Anatomy made many pictures. It records images of the recording space around the development. Then segmentation images and the possibility of the Atlas, and employment in the field of Bayesian average. The

possibility that belongs to a particular device for each pixel / voxel is calculated. Finally, the use of simple threshold or algorithm to extract the target device based TRS police perspective. The problem is that the possible generation of the Atlas needs to a large amount of training data to be collected and pieces.

In [14] they hired a rigid implementation of the liver Atlas. Atlas 20 education is provided from the image to capture two images for the construction of the Atlas. The first step is to turn affine to use mutual information (MI) measured by [17]. At the time after the registration of the *B-firm-Mills* by [18] using a combination of MI, and death cost ration surface the relevant section is proposed. At registration, each training image of all the others, and the average deformation map thus converting all images to the coordinates system. On average, every image and piece can become the ultimate atlas image. Image segmentation, testing, and user-defined affine to convert almost matches the image of the Atlas. After optimization of the affine transform, the user specifies what the atheist E on the liver of the registration Name of non-rigid later. At this point, hiring the same way during the construction process of the Atlas, but without the distance of death. Use the correct shape and thus become the Atlas division of imaging test. This division is 50% threshold and morphological open operations proposed by [14] and remove it from the elements joined after the final result.

3.5.2 Fully automated liver segmentation method

This fully automated liver segmentation in its T is described. The term “fully automated” means that it will not divide the liver and run without any operator intervention. In general, this type of approach is highly appreciated by the radiologist to user error free and ES Bahrain Insurance Association, and it provides the operator of the hard work and potentially a lot of time is wasted.

3.5.2.1 Automatic method based on deformation model

In [19], I developed an appropriate model for liver and kidney parameters 3D a way to adapt to abdominal CT images. In this approach to conformity assessment between the definition of slope deformation and image. Unity normal level getting better coordinate

the energy function to a minimum. In evaluating the results of the division of the liver by visual radiologists, while object uses the measure to assess the division right kidney. In order to describe a complex form of the liver using the transformation model, one should be limited to the value of strong global constraints and intense noise. This explains the reasons in many cases for the lack of diversity in the natural liver. Researchers, in [20] and [21], with the aim of overcoming this limitation by using a hybrid approach, combined with the deformation of the flexible recording technology.

3.5.2.2 Statistical Model C control method

Form statistical model has made a series of examples of the form. Representation in any form of education is determined by a group of n tag salient points. The alignment of training samples described in a common Framework for Coordinated by procreates analysis. The latest unsaturated, rotation and scaling all training to minimize the total distance to the square of the average range.

In [22] the liver is divided by SSM as a way to achieve a high robustness to noise and extreme value. The method draws a map of the half to build the model to be used. In this way, user interaction is required to mark the corresponding points in all training data P vibrant as the main component analysis (PCA) with training data used to capture changes in the liver form. After that allows model deformation space in the arrest of differences, through the implementation of personal information by [59].

The method proposed by [60] related to the SSM data and image distortion correction solutions using the network. SSM consists of approximately 7,000 signs and made from a wide range of training 112 forms of liver. By correspondence needed using a semi-automatic mode, where it appears on the surface characteristics of the vertical run in all parameters can be determined. This is the position heuristic Jim liver limit per definition has been estimated. This classification recruitment process specific density of the liver and tumor models, on behalf of any intensity are. Borders are calculated using the voxel intensity graph in the current division of the liver. The amount of processing Gaussians this graph with the expectation-maximization (EM) algorithm proposed by [61], and derived from means is obtained and the standard deviation limits. Before you start sector, and aligning images using non-linear release properties

provided by [24]. A form of SSM, as the lobe of the right lung using a threshold and morphological processes by [25] is known. Diagnosis then the first piece that contains no lung lobe is expected to voxels, and the center and going to drop below the initial development of the SSM. In [26] it is in the context of different algorithms proposed by [27], which follows the divisions SSM step which is distortion free. The sample consisted of 50 samples provided by the functions of the remote site. And not a sign of concern, and determining correspondence is not necessary. The authors distributed in the form of non-parametric kernel density estimates provided by [28] is used. Create SSM, and chart analysis and image compression using a Gaussian model are mixed. Where works of the liver tissue density of the threshold image analysis. Pixels based on the yields the highest response in image of the mask into the liver so it is a lie and as a starting point for the development of the Group used.

3.5.2.3 Atlas in the way of possible mechanisms

The approach proposed by [29] in the classification of voxels in the country of estate with multiple log Atlas. K nearest neighbor (KNN) to label each voxel in the region nominated automatically detect liver or background. In the process, every image voxel R for sample E is isotropic. To identify and correct the rotation axis Z, it was revealed bones and the maximum threshold of the binary mask that through the use of different periods. After that, the lungs through the threshold and potential liver area to a steady increase in all parts of the lower edge of the nozzle is limited lung. After ten scans recorded training specific to the new image using affine transform followed [32] in multiple resolutions. To this end, the negative information on labor costs [33]. Indicator stochastic gradient optimization exchanged offer. With developments leading to individual training divisions map new image. The production division probabilistic atlas [34] is based on three characteristics of the space: it represents the percentage of high risk fragmentation, left, behind the voxel in question. After all voxels in the vicinity of a G-Class Masks with the nearest neighbor record 15, after the announcement of the results by homogenous morphological operations proposed by [62] processing.

3.5.2.4 Automatic methods based on cultivation

Works cultivated area developed by technology [31]. In his research, and the intensity graph to estimate the distribution of density analysis of the liver. And above and below the threshold value into a mask image binary, which is used at a later time with a large nucleus. This process leads to an isolated area in the center of the liver as the seed for the cultivation area after it is used. Once again, the estimated distribution density of the liver is the seed region, and it is added to the adjacent voxels within a radius of 5 mm voxel me and every density is estimated at a distance to prevent leakage at the heart of regional growth, which has been linked to the lower parts of both early detection of lung lobe and the mind. After treatment, the atheist and the right lung lobe are on the border, and the distribution of new voxel intensity estimates is not classified until now, according to the region Second place in this area has been limited growing. After that, the leakage through the vena cava by citing half a predetermined period right circle at some point and delete slides in diameter if they meet the standard required length. And works with smaller labels as liver tumor vessels and cavities of trees. In the end, it turned to a net binary mask, smoothed, and the original data have become voxel decision. Collect and classify voxel, the EM algorithm and cut liver in CT images by setting [64] growth area. And EM uses an algorithm to determine the confidence of the distribution of air density, and fat - tissue soft bone in the training images is available. With this amount of density and the decomposition tree four separate each part of the image is analyzed tissues and tissue regions. All regions of texture, fabric Haralick calculation features [64] and their classification and regression tree [65].

3.5.2.5 Qaeda based on automatic

In [66] they specialized programming language to define a set of rules that are used to extract different structures of test images hire. The order is obtained after air field, the lungs and the air inside the body, and the subcutaneous fat layer and muscle and bone in the layers of muscle, and aorta, spine, heart. Any additional C stepwise, the system makes use of detection structures is present to help analyze images. Rules can knowledge about the distribution density, neighborhood relations, integration, and

engineering features, etc. After the extraction of these structures of the heart, the liver by the right of the selected area of the grain before undergoing cardiac CT slices, until the diagnoses achieve the object of a certain size. From these seeds in the region, a process similar to (but not including surface image smoothness constraints), the growing region. The growing trend of the ban by some previously undiscovered structures within fat, and by others as lung absorption (allowing the liver, lungs grows to restrictions). All the rules without the use of training data that are systematically applied image is not optimal parameters.

3.5.2.6 Automatic method based on gray level

The methods in this category in the statistical analysis of the CT are according to manually split the liver in order to estimate the level of gray. Some of the other methods used in the analysis based on the information before the chart. This book Lim et al. [66] liver segmentation method based on the idea of the mechanism defined above mention suggested researcher's study the formation of liver CT density distribution of fragmented manually. Using previous information about the site hepatic extraction of the primary liver size of the political analysis of CT image slice of manually extracting information. Then, algorithm K - almost and morphological liquidation to get rid of connected devices to the liver, liver border recognition is to enable the program to smooth the liver restrictions on the exercise of the slope, and the density distribution, and liver pattern features. In [67] They hired a feed-forward neural networks with the support agnation back on the liver and liver and non-liver border of the images trained, while [68] using the Hopfield neural network without censorship, Photos and a set of features Horlicks input image texture. Both methods tested using only a picture of the performance is very low. In [4] promising results when used text URE neural networks and methods based on pixel gray levels and location information to recognize and separate the different control devices are obtained. Seven fuzzy rules based on location, size and shape of each border refined hardware device form an image based on relationships between subsequent images. When the two share a close neighbor and gray levels, a chance to increase system failure suffered. Second, using no force in dealing with various forms of binary

data on employment law and Q phase experimentally determined value of the rules is limited.

3.5.2.7 Level Sets

The level sets is considered another widespread method in the process of segmenting the medical images. It is considered as the growing contour that can modify the topology. We can think the level sets as a circle that be located in the image, and this circle can expand in stable average and can be stopped by the image edges. It can be separated in different direction and when two edges have been met they will be merged in a single edge and remain in this mode. This capability on merging and segmenting can help the level sets on splitting the object on high category. The group of the curves can form the R surface that called the function of the level sets. Through moving the plane image up and down with respecting the surface, the resulting changing-shape that will be produced will be the intersection between the plane image and R and the contour will be formed that been illustrated above.

The level sets techniques that will be able to modify the topology will be very effective to splitting the soft tissue because it will be able to dealing with cavities and the merge and segmenting process that usually found at this tissue. For instance of these objects are brains, arteries and veins. Nevertheless, one of its requirements the object's edge should not be broken. According to the features and the nature of the level sets approach the contour will suffer from the outflow of the gaps resulting in unsuccessful splitting process for the element or the required object. This is dissimilar active contours that be reserved by inner forces. Moreover, the preliminary situation to the original contour will be very essential. The mistakes in placing may resulted of the segmentation of very few parts of the required object or further objects have been split. Yang et al., [69] combines the information of the statistical area in the elementary level set forms to develop the strength of the segmented medical images and that will increase from the accuracy of splitting the image with fuzzy or fragile edges. In addition, Chen and Tseng, [70] have used the statistical information on the format of Bayesian risk hypothesis to achieve the segmenting process to the noisy image that consist on low contrast. Moreover, Cremers et al., [71] have executed a review on the

level sets that consisted of incorporating statistical information. These applications suffered from the need of extracting information from the training models because it is more powerful than the level sets form. Finally, it may be there are difficulties to get the training sets form for efficient sizes in order to obtain statistical information with meaning.

4.5.2.8 Edge-based

The edge-based approaches endeavor to discover the places of fast transition from one region to another for different values of color or brightness. The basic standard that edge-based works on is to apply some of the gradient parameters that is found in the image. High values from the gradient sizes can be puted for the fast transitions through two different regions and these regions called the edges. After the image edges have been found these edges are connected to configure the closed borders for regions, and the process of transition from the image edges to the image borders is a very complicated process. This technique can be beneficial from the discontinuity of borders and through it can extract the contour of the interested region. As well as, this approach is useful to segment the image because the edge denotes confluence for two neighboring regions. Edge-based methods look for the contour along which there is a change in the differentiating characteristics beside the regular of the contour. The contour is known as the edge and the most important topographies that use by this technique are the color, intensity and the texture. Brejl and Sonka, [72] has been segmented the ultrasound medical images through merging the machine learning with the edge-based. The results that Godbole and Amin, [73] have gotten through their method is being compared with the manual segmentation that's been done by the experts. Godbole and Amin, [74] have detected the interference in the edge through the use of mathematical morphology to the lung images that been taken by the camera of the gamma ray. The core advantages of using mathematical morphology are its robustness and its ability to execute it on the hardware devices in order to realize the real speed time.

Furthermore, Liu et al., [74] has invented a method to use the morphological in order to implement the process of detecting the edge for the wall of the heart ventricular by using the ultrasound. Edge-based segmentation method is common to use it in the pre-processing step in the more developed segmentation algorithms, for instance, active contours, level sets and atlas-based segmentation. Moreover, the edge-based is considered a very useful method in several cases especially when the image contains noisy and high contrast through the objects in the image. Nevertheless, the medical image is always contains noise in addition to have poor contrast between each two organs.

CHAPTER 4

PROPOSED SYSTEM

4.1 Introduction

This work aims to build an accurate semi-automatic system to determine the region of interest from a human body followed by computing the region volume. As mentioned previously, any system can pass through several stages and many techniques can be used in each stage. These methods will play great role in realizing the system accuracy. Consequently, the system that's been proposed focused mainly on the enhancement phase that in turn effects on the segmentation results.

4.2 Proposed System

This thesis mainly introduces a system to compute the liver volume from computed tomography (CT) image enhancement techniques that eliminates noise and obtains a better image contrast in order to segment a suspicious region. This section explains in detail the stages of these system techniques of a segmented image in computed tomography (CT).

In the first step, the Adaptive Histogram Equalization (AHE) and threshold has been applied to enhance the edge and content of the tomography (CT) image so as to be ready for use in the segmentation process. Image segmentation very effective in maximizing system accuracy. In this step, region growing and edge detection to segment the image is used after which we apply the morphological algorithm to fill holes resulting from segmentation .Once the answer is obtained, we compute the liver volume.

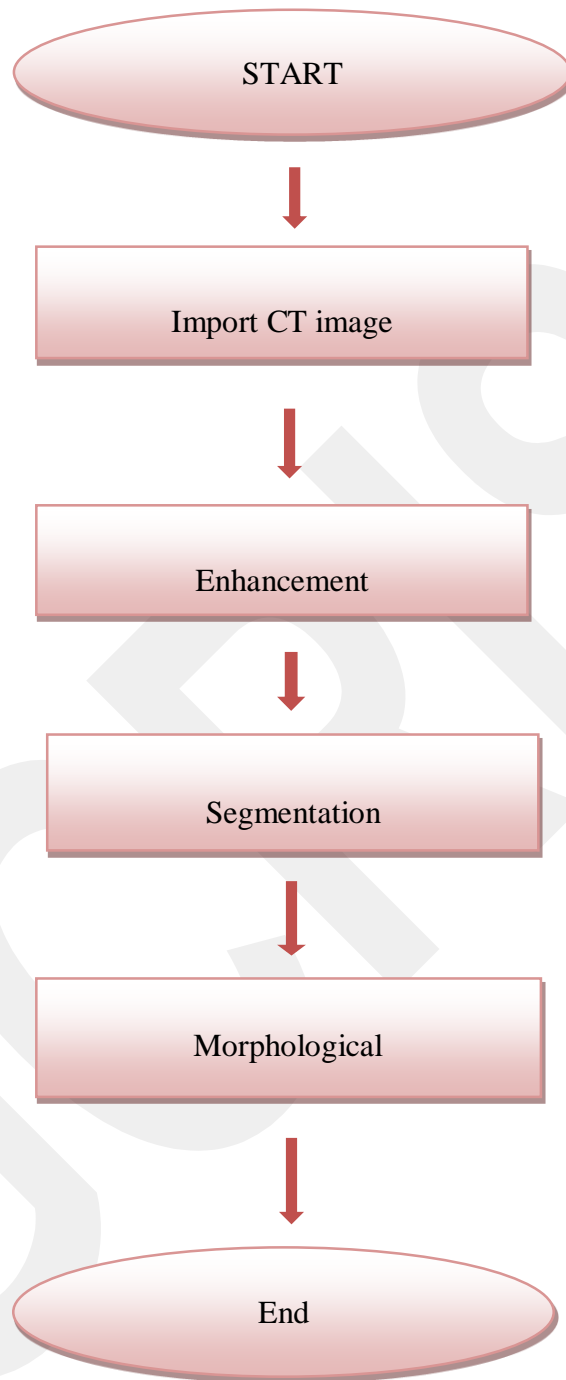


Figure 9 Flowchart Diagram of The System

4.2.1 Image Enhancement

In order to enhance the image the main thought is to deliver an improved subjective realization. The main purpose of image enhancement is to strengthen the edges or the image characteristics with keeping better edges or features, as well as, to eliminate the noise.

4.2.1.1 Thresholding

Threshold can be implemented easily on both the frequency domain and the spatial domain. The thresholding can be applied complemented with image processing applications for different aims and the threshold can be defined as a means to separate the image in preliminary form. The threshold of the image can be applied in order to separate some region in the image from its background to get the separate characteristics, if that region in the image is separated from the intensity level. Nevertheless, due to the contrast that be in the tomography (CT) image, it is challenging to recognize gray levels that belong to pixels which denote micro calcifications. Also, the other thresholding applications is to reduce the noise. Through the thresholding the noise of the image can be detected in both the frequency and the spatial domain. The image is considered as a noisy image if the threshold value T is less than the assigned threshold value.

$$g(x, y) = \begin{cases} 0, & f(x, y) \leq T \\ f(x, y), & f(x, y) \geq T \end{cases} \quad (4.1)$$

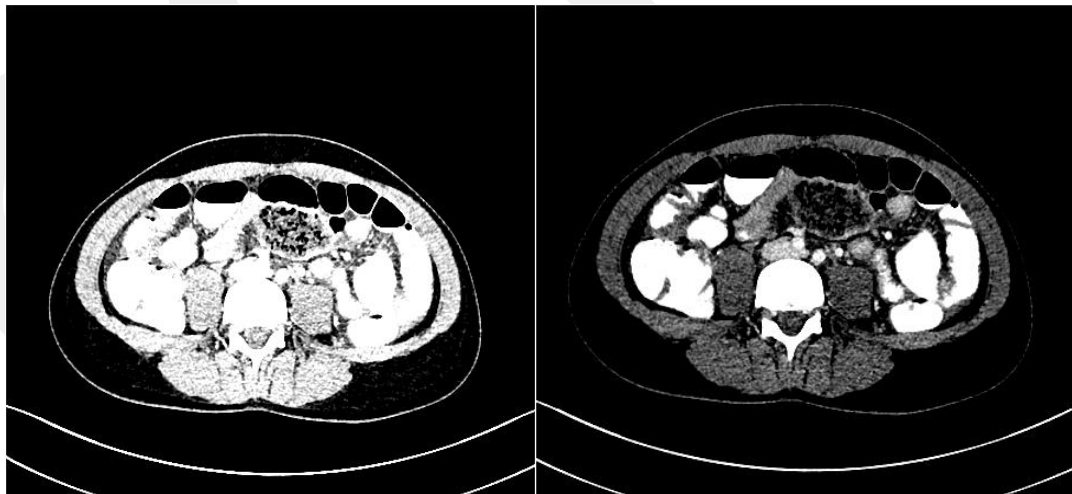
In this thesis, the threshold value has been used in order to integrally enhance the image with other image enhancement approaches.

4.2.1.2 Histogram Modeling by Adaptive histogram equalization (AHE).

One of the most common approaches to enhance the image is the Histogram equalization (HE). A histogram of an image accompanied with the levels of the gray which located in the range $[1 L-1]$ denotes the number of pixels for every gray level. Moreover, through the image histogram equalization we can obtain information about the contrast of the image and the noise information such as the salt and pepper noise. Through the histogram equalization we can enhance the contrast of the image in the spatial domain with less calculation cost as compared with the frequency domain applications. Moreover, they can offer images which have high contrast with the huge dynamic set of the intensity scale. The model of adaptive histogram equalization has been used in this thesis.

$$I(x,y) = f(i(x,y)), DN(x,y) = f(N(i(x,y))). \quad (4.2)$$

$N(x,y)$, the contextual region, is some spatial neighborhood of (x,y) in the image that contains the pixel of interest and $DN(x,y)$ is some group of measurement over $N(x,y)$.



A

B

Figure 10 (A) Image of CT scans before enhancement
(B) Result Image of CT scans after Applying (AHE).

4.2.2 Segmentation

This stage involves using two techniques to segment (ROI) and includes a lesion to extract it from the enhanced image which was obtained from the previous stage.

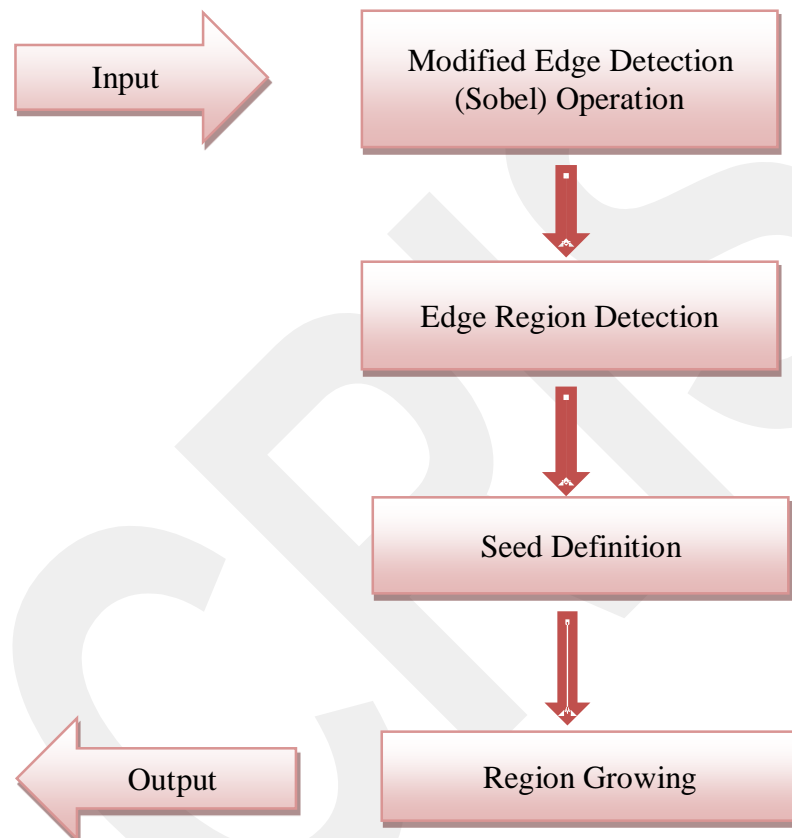


Figure 11 Sub steps of Segmentation Process

4.2.2.1 Edge Detection by Using Sobel Operation

It could restrict the numerous methods that are used to detect the edges of the image into two main groups are the gradient and Laplacian [75]. The method of detecting edges by using gradient technique is looking for the minimum and maximum in the

first order derivative of the image, whereas, the Laplacian technique is finding the image edges by searching on the zero principles in the second order derivatives of the image. Also, the edge detection technique is one of the most common methods which is used to detect the important discontinuity in the values of the intensity. These discontinuities founded by the first and second order derivatives. Furthermore, the gradient technique is considered as first order derivatives that been chose in the image processing techniques. However, the Laplacian method is used rarely in order to detect the edges because it is in the second order derivatives will be sensitive to the noise in unacceptable form. The laplacian will produce a magnitude with two edges and will be unable to detect the direction of the edge. What follows is the edge detection techniques: The Sobel operator executes a 2-D spatial gradient measurement on an image thereby highlighting regions of high spatial gradient that match to the edges. It is typically used to find the size of the absolute gradient in every point in the gray image scale that been input. In addition, the Sobel method is considered as a simple detector for the vertical and horizontal edges for that it uses it this case the H1 and H3 masks.

$$H1 = \begin{bmatrix} 1 & 2 & 1 \\ 0 & 0 & 0 \\ -1 & -2 & -1 \end{bmatrix} \quad H2 = \begin{bmatrix} 0 & 1 & 2 \\ -1 & 0 & 1 \\ -2 & -1 & 0 \end{bmatrix} \quad H3 = \begin{bmatrix} -1 & 0 & 1 \\ 2 & 0 & 2 \\ -1 & 0 & 1 \end{bmatrix}$$

Figure 12 Sobel Edge Operators

If the H3 response x , and the H1 response is y then the edge magnitude (strength) is

$$\text{Magnitude} := \left(\sqrt{x^2 + y^2} \right) \quad (4.3)$$

$$\text{Direction} := \text{inv} \tan y/x \quad (4.4)$$

The Sobel parameter is considered slower but its detour mask is bigger as compared with the input image and that will make the parameter more sensitive to the noise.

Furthermore, the operator is always producing output values and is considered high for the similar edges as compared with the other approaches.

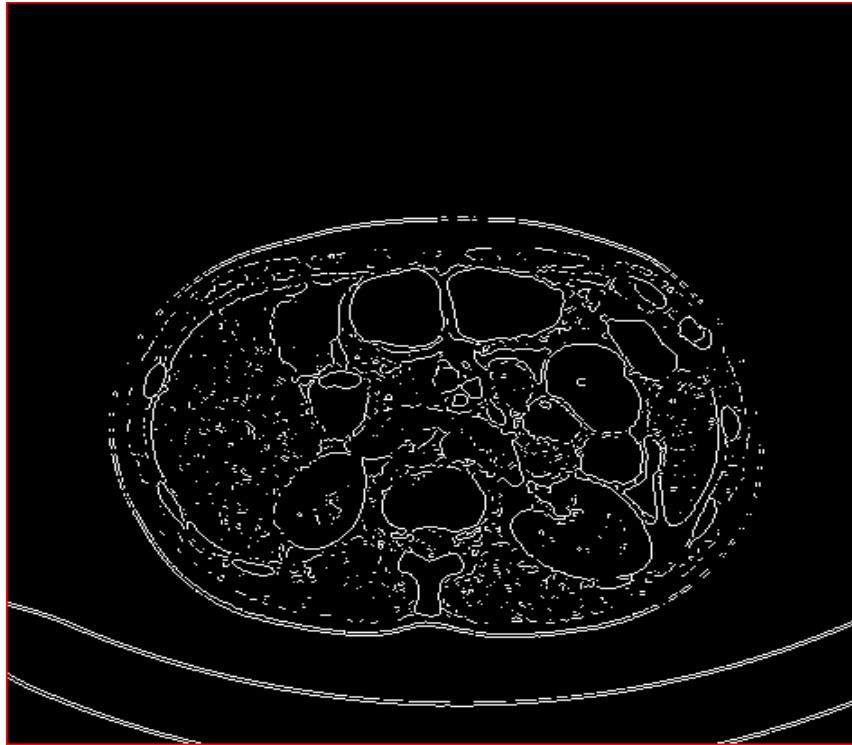


Figure 13 After Applying Sobel Edge Detection

4.2.2.2 Segmentation based on Regions

The primary goal of image segmentation is to transform it to regions. A number of segmentation approaches, for instance, those based on a “threshold,” are able to achieve this, by seeking the boundaries between the various regions on the basis of color properties or on discontinuities in gray levels. The regions based segmentation is a method that directly determining the image. The main formulation of the segmenting process depends on regions:

- (a) $\bigcup_{i=1}^n R_i = R.$
- (b) R_i is a connected region, $i = 1, 2, \dots, n$
- (c) $R_i \cap R_j = \emptyset$ for all $i = 1, 2, \dots, n.$
- (d) $P(R_i) = TRUE$ for $i = 1, 2, \dots, n.$
- (e) $P(R_i \cup R_j) = FALSE$ for any adjacent region R_i and $R_j.$

$P(R_i)$ is a predicate function defined on the points overall $P(R_k)$ and \emptyset is the null set.

(A) Refers that the segmentation process should be finished and each single pixel should be in one region.

(B) That is required that the points in one region should be linked in some way by default.

(C) Refers that the regions should be separate.

(D) Relates to the characteristics that must be fulfilled by the pixels in the segmented region. For example, $P(R_i) = TRUE$ if every pixel in R_i has the same level of gray.

(E) Refers that the region R_i and R_j are different in the common sense of the predicate P .

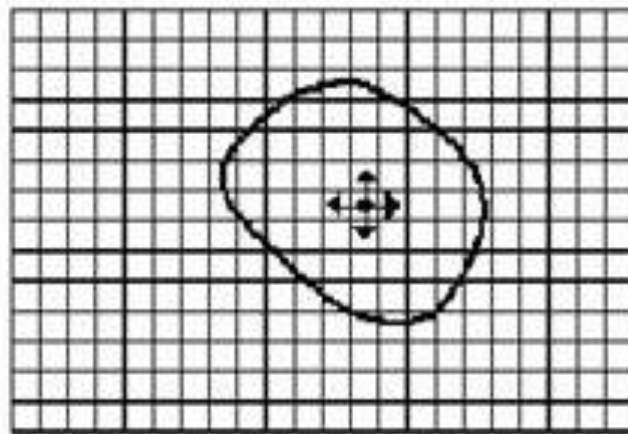
4.2.2.2.1 Definition of Region Growing

This technique segmented the regions by the data volumes, where the user can choose a point and region growing from the seed point until execute some of the standards of growing stopping have been stopped. The region growing usually creating one region used to separate one object, for instance, the data volumes may contain on dissimilar objects and can be separated by the threshold. Later, every single one of them might be separated, whereas, the region growing will separate only the object from its seed point.

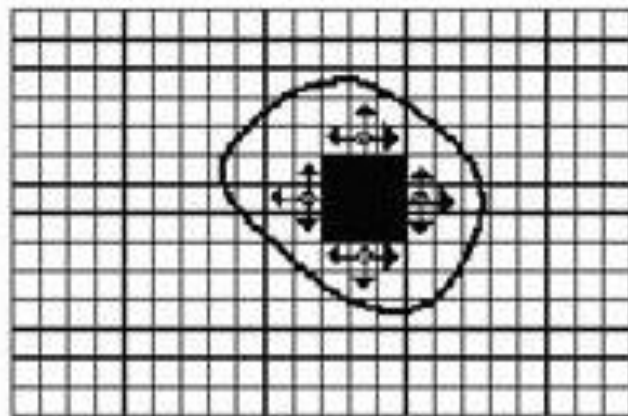
4.2.2.2.2 Basic Region Growing Approach

This approach is considered an opposite method to the merge and split method [76]. Where a small set of regions has been merged repeatedly according to the matching restrains. The seed of pixel been selected and compared with the adjusting pixels as illustrated in figure 14. Thus, the region is growing from the seed pixel by adding the adjust pixels to it and it should be similar and that will increase the size of the region.

When the growing process being stopped another seed pixel will be selected which does not belong to any region been selected and the same procedure will be repeated. This process will continue until every single pixel will belong to one region.



↑ direction of growth • seed pixel
Figure 14 Start of growing a region



■ grown pixels ○ pixels being considered

Figure 15 Growing process after few iteration

4.2.2.2.3 Geometric Characteristics of Regions

The primary goal of the region growing is to use the features of the images to mapping the individual pixels in the input image to a set of pixels known as the region. Also, each region has geometric features depends completely on the domain. Moreover, the geometric characteristics should be linked to two dimensional region. It does not matter if the regions are not connected and separated, the borders that belong to that region should be smooth and that feature relies mostly on the region growing techniques and on the work goals. Finally, the main principle of the segmenting process is to segment the entire image to almost separated regions, i.e. to non-overlapping and 2-dimensional regions and that region does not contain any pixels that belong to more than one region.

4.2.2.2.4 Basic Concept of Seed Points

The process of selecting a set of seed point is the first step in the region growing method. The process of selecting a seed point depends on certain criteria established by the user (for instance, pixels equally spaced on a grid, pixels belonging to a several range of gray levels, etc.). The seeds represent the exacting position of the initially started regions. Then, these regions are enlarged from these seed points to the other neighboring points in accordance to the standards that belonging to that region. The standards may be for instance, the level of gray, the color or the pixel intensity. The information that belongs to the image is very important because the regions are growing according to the standards that been used. For instance, if the standard was to use a threshold of the pixel value, knowledge of the histogram of the image would be suitable to decide a threshold value suitable to the standard that's been used.

A very simple example is described below. If we consider 4 pixels adjacent to the seed point and the criterion used is that of similar value of the pixel, i.e. We examine the adjacent pixels of the seed points. If it has the same value in intensity as the seed points, we classify them as seed points. The iteration steps will continue until no changes happen in the two subsequent phases. Moreover, it is possible to use another technique but the main goal is still to classify the regions similarity with the image being used [77].

4.2.2.3 Integrating Region Growing and Edge Detection

This method is used to merge the edges that exist in some region been detected by using the optimal edge parameter. The edge of the region is defined as the place which will be used to select the growing seeds. Thus, the region edge must be adjust to the pixel edge that been derived from the edge parameter. Later, the region size will be compared. Moreover, the highly small areas will be removed from the region edge in lieu of being merged. Then, the effects that being caused by the noise will be completely removed. Later, the image will be segmented into two types of regions. The first region will be called the edge region and the other is called the homogenous region. In our study, firstly, we performed edge detection is performed, followed by edge region detection and lastly seeded region growing.

In some frames, some sections are segmented mistakenly. In order to avoid, we cut manually and this part is considered for other frames. For example, in Frame 80 after segmentation, we obtain the result as shown in Figure 15. At this time, we select the extra part of this segmentation and this state is shown in Figure 16.

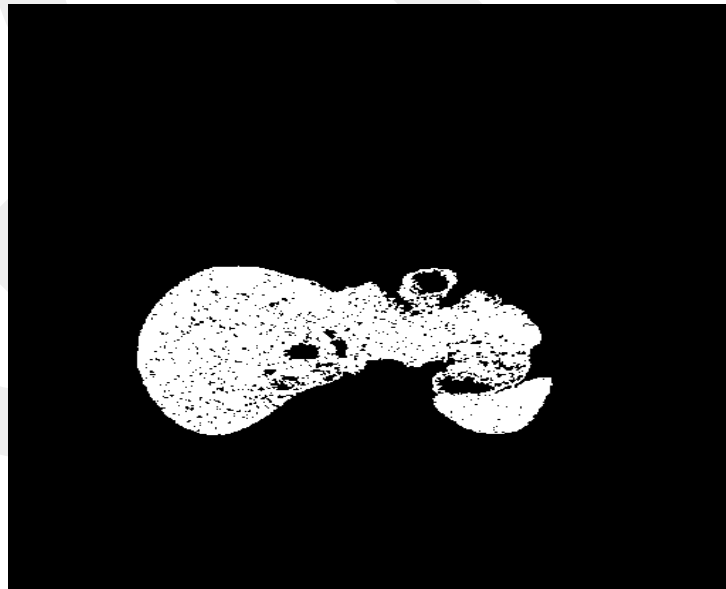


Figure 16 Frame 80 after segmentation

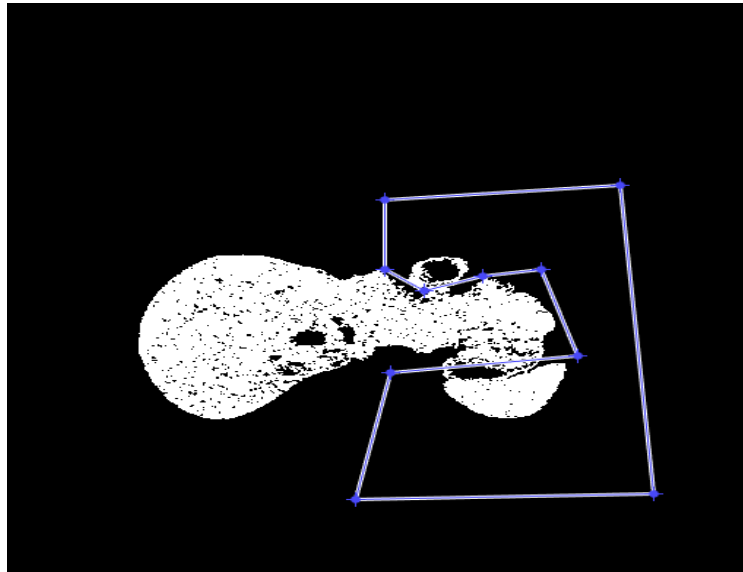


Figure 17 Selecting of the extra part of segmented place

After selected the extra part the result is shown in figure 18.

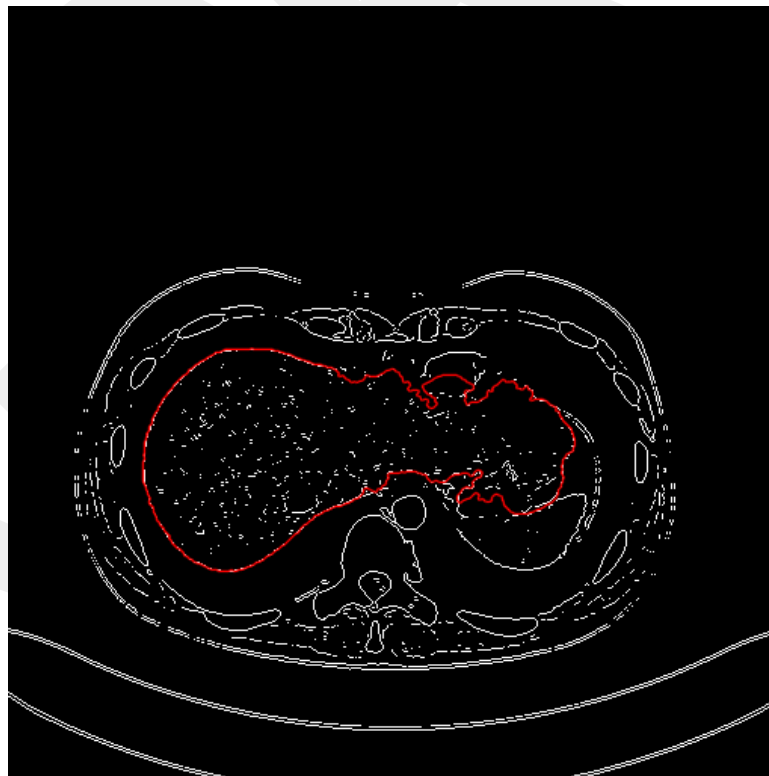


Figure 18 After selected the extra part

4.2.3 Morphological Algorithms (Hole filling)

After obtaining the answer, the image has some noise. We used the morphological Hole Filing algorithm to eliminate the noise. The morphological algorithm was applied to fill any holes. Moreover, the hole is defined as the background of the surrounded area that linked to the boundaries of the foreground pixels. Through this section, the algorithm depends on the set of dilation, complementation and intersection to filling the holes that are in the image. If we assume that A represents a set where its elements are 8 associated borders, then every border is accompanied by a background region (i.e., hole). Assumed a point for each hole, the aim is filling each hole with 1s.

We begin by creating an array, X_0 of 0s (the similar size as the array holding A), excluding the positions that correspond to the specified point in every hole, that's set to 1. Formerly, the procedure follows will fill each hole with 1s:

$$X_k = (X_{k-1} \oplus B) \cap A^c \quad K=1, 2, 3, \dots \quad (4.5)$$

Where B is the component of the symmetric structuring. The algorithm will terminate at iteration step k if the set then encloses all the filled holes. The union set of A will contain all filled holes and their borders. The dilation in Eq. (4.5) would fill the entire area if left unchecked. The result is shown in Figure 19.

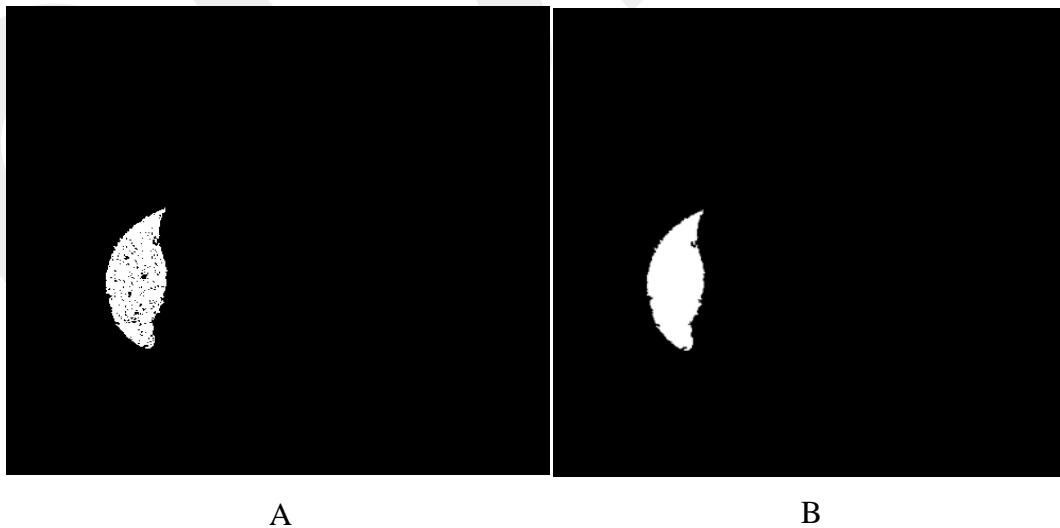


Figure 19 (A) Image before applying Morphology, (B) Image after applying Morphology

4.2.4 Calculation of Liver Volume

The algorithm will retrieve the thickness of the slice (in mm) and the spacing between the pixels (in mm) from the header of DICOM for the series of the image that be through the processing to calculate the size of the liver using (4.6).

$$\sum_{i=1}^N A_i T = \sum_{i=1}^N S^2 P_i T \quad (4.6)$$

NN denotes the overall number of ROIs of the liver that composes the model of the liver. AA_{ii} is the area of every ROI ii and computed by using the spacing of the pixel SS and the entire number of pixels PP_{ii} of every ROI ii while TT is the wideness of the slice every image. Moreover, the formula is applied when computing the size of every split liver.

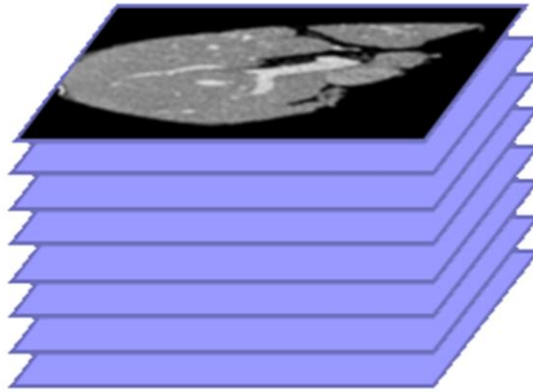


Figure 20 CT image series (a sequence of slices)

CHAPTER 5

EXPERIMENTAL RESULT

5.1. Overview

This chapter first discusses the results that were taken from the proposed method. Secondly, it also deals with the results that were obtained from the images after enhancement. In other words, it examines a segmentation part of the area taken from the images, finally followed by comparing between the results before and after while processing Liver form differs from slide to another in some slides are big and some are small and some are not clear overlapping borders with other member

5.2 Data Set:

Through our study, we have used the CT data and one patient (WOMEN, age range). The scanning parameters included a slice thickness of 1 mm. Each CT slice had a matrix size of 512×512 . The radiologists have been traced the manual liver contour carefully on every slice covering the liver. At this case, the slices number ranged from 50 to 324 slices. The pixel spacing is 0.75×0.75 for each slice. The size of the liver has been computed by multiplying areas of manually traced regions in every slice by slice thickness and pixel slicing. Thus, by doing the summation operation of the sizes in each slice we get the size of the whole liver. The scheme that we have calculated it has been evaluated using the manual liver size that considered as a reference standard.

5.3 Experiments

By using MATLAB R2015a, this semi-automatic system was built on a computer with the following components:

- Microsoft Windows 8.1 Enterprise 64-bit.

- Processor: Intel® Core™ i5-3210M [CPU @ 2.50 GHz](#) 2.50 GHz.
- 6GB RAM.

In this experiment, we have tested our approach on a computed tomography (CT) image. The first step prepares the image for ROI segmentation by applying image enhancement techniques. Figure 20 (B) Frame 55 after Enhancement and Figure 23 (B) Frame 100 after enhancement show the results after applying the remaining enhancement techniques. The second step is segmentation; in this step of the system used edge based and region based Figure 21 (A) Frame 55 After Edge Based (B) Frame 55 After Region Growing and Figure 24 (A) Frame 100 After Edge Based (B) Frame 100 After Region Growing. show the result after applying edge detection and results after applying region growing. The last step is a morphological operation to fill holes. Figure 22 (B) Frame 55 after the morphological operation and Figure 25 (B) Frame 100 after the morphological operation show the result after applying morphology.

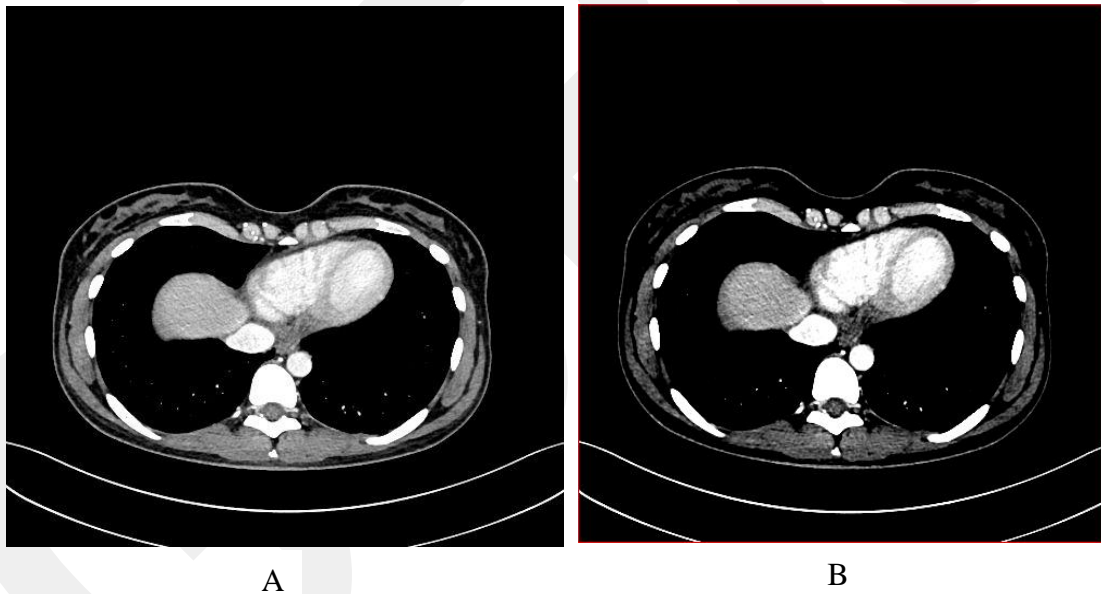
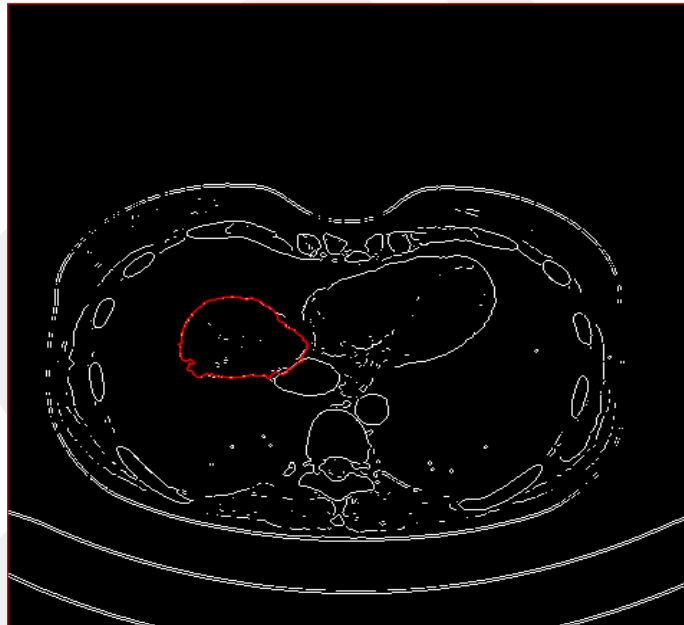


Figure 21 (A) Frame 55 Original Image, (B) Frame 55 After Enhancement



(A)



(B)

Figure 22 (A) Frame 55 After Edge Based, (B)Frame 55 After Region Growing



(A)



(B)

Figure 23 (A) Frame 55 Segmented Image, (B) Frame 55 After Morphological Operation

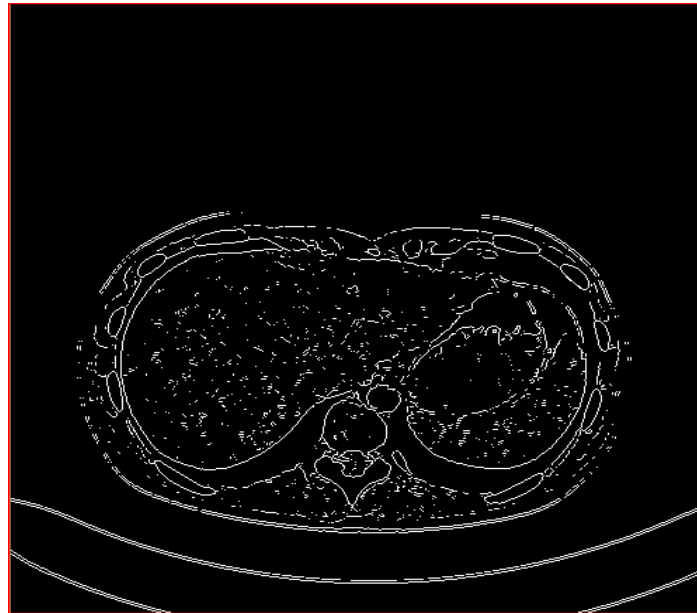


(A)

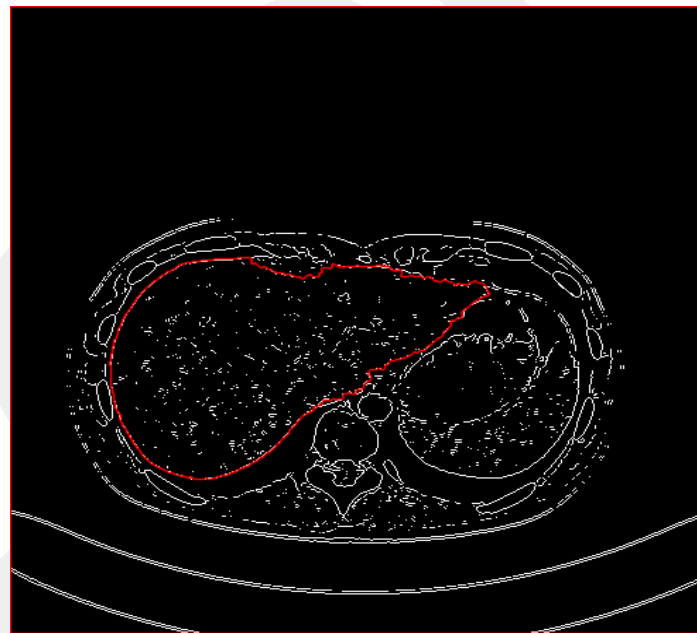


(B)

Figure 24 (A) Frame 100 Original Image, (B) Frame 100 After Enhancement

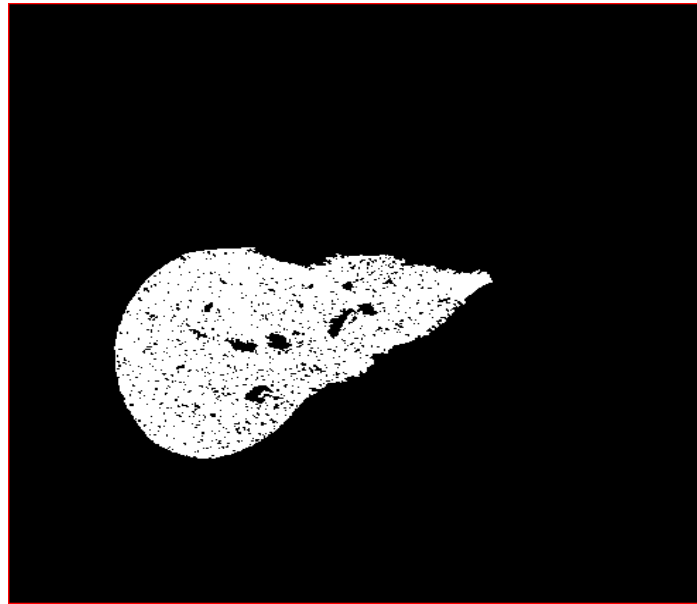


(A)

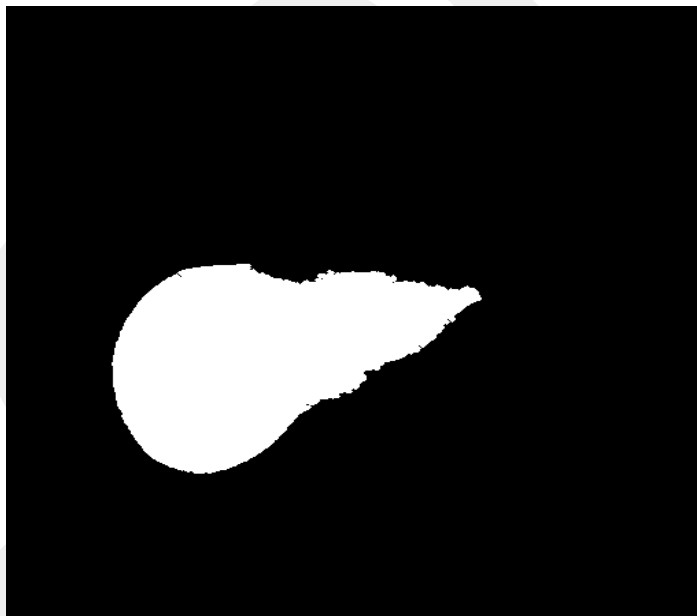


(B)

Figure 25 (A) Frame 100 After Edge Based, (B) Frame 100 After Region Growing



(A)

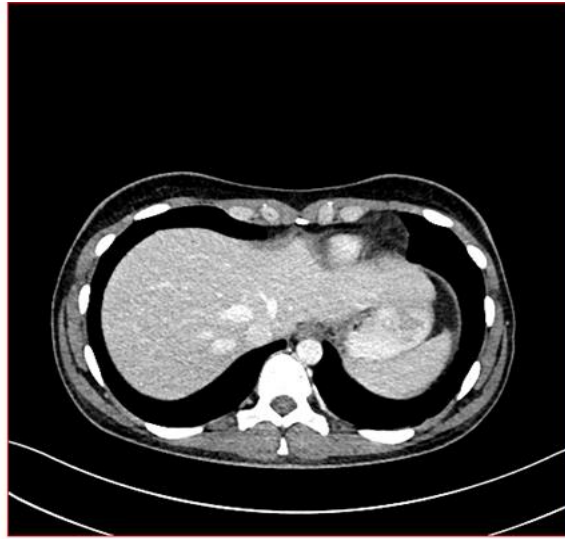


(B)

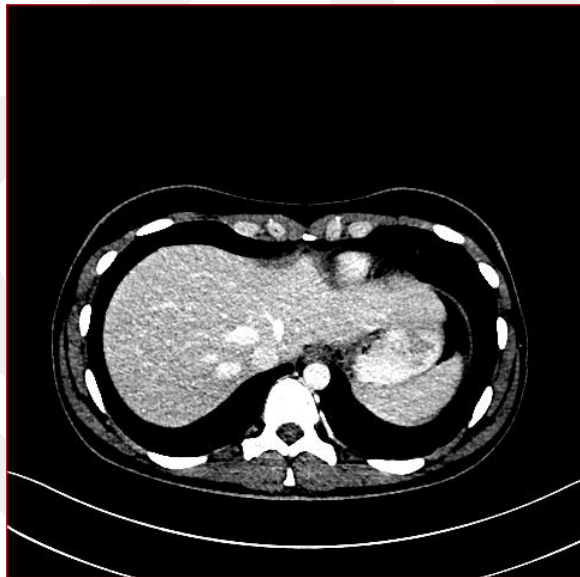
Figure 26 (A) Frame 100 Segmented Image, (B) Frame 100After Morphological Operation

The basic difficulty that we have faced in this study that is the intensity of the liver is highly similar to the intensity of the organs adjacent to it like the stomach and the spleen. Moreover, sometimes is impossible to recognize it even with the existence of the visual perception. Also, the information of the edge in the abdomen is very complex.

The complication of edge information in the abdominal image is shown in figure 27.

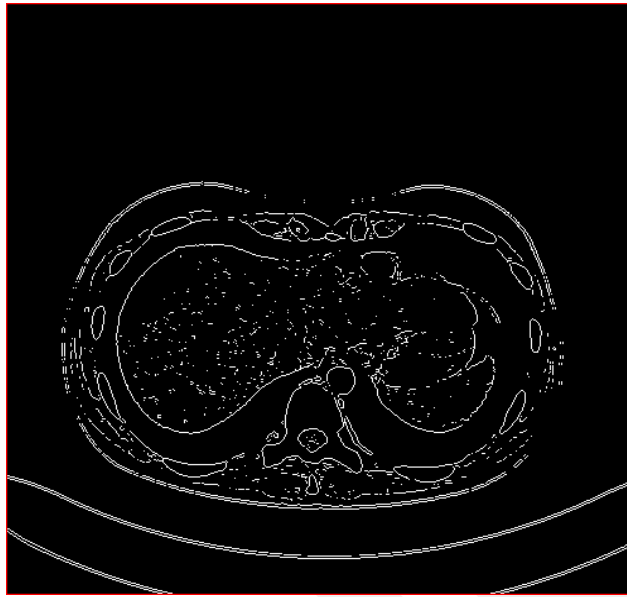


(A)

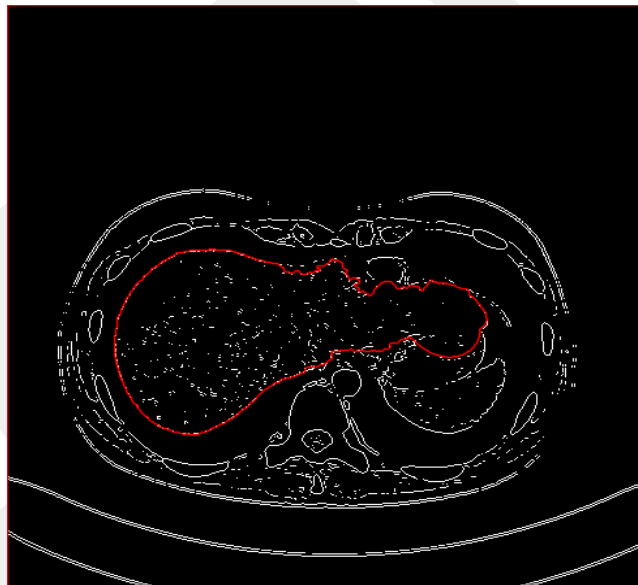


(B)

Figure 27 (A) Frame 83 Original Image, (B) Frame 83 After Enhancement

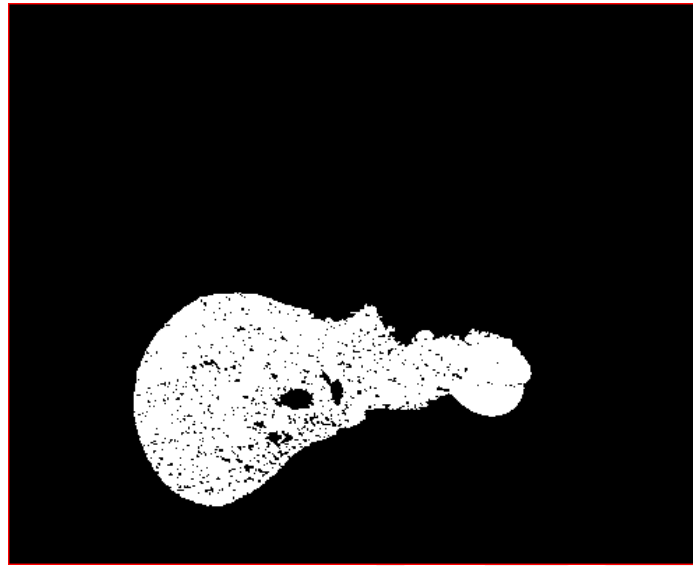


(A)

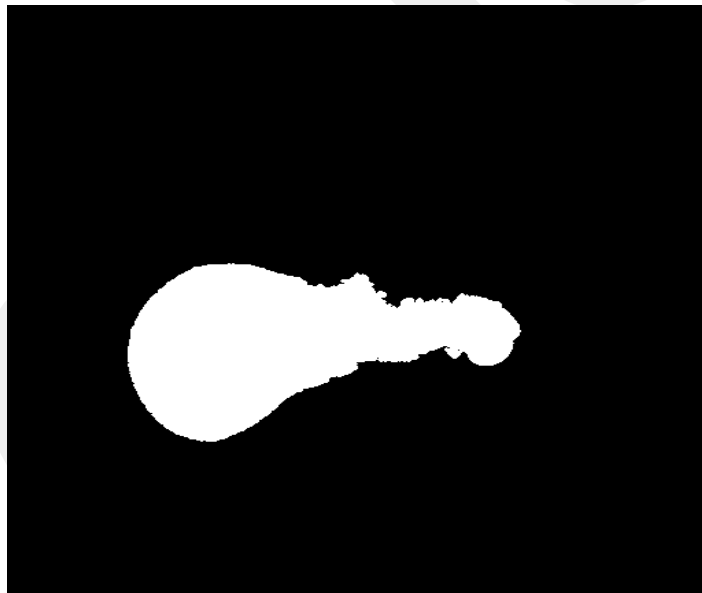


(B)

Figure 28 (A) Frame 83 After edge based, (B) Frame 83 after region growing



(A)



(B)

Figure 29 (A) Frame 83 segmented image, (B) Frame 83 after a morphological operation

In some frame some section is segmented mistakenly for avoid of this reason we cut manually and this part is considered for other frames. For example in Figure 30.

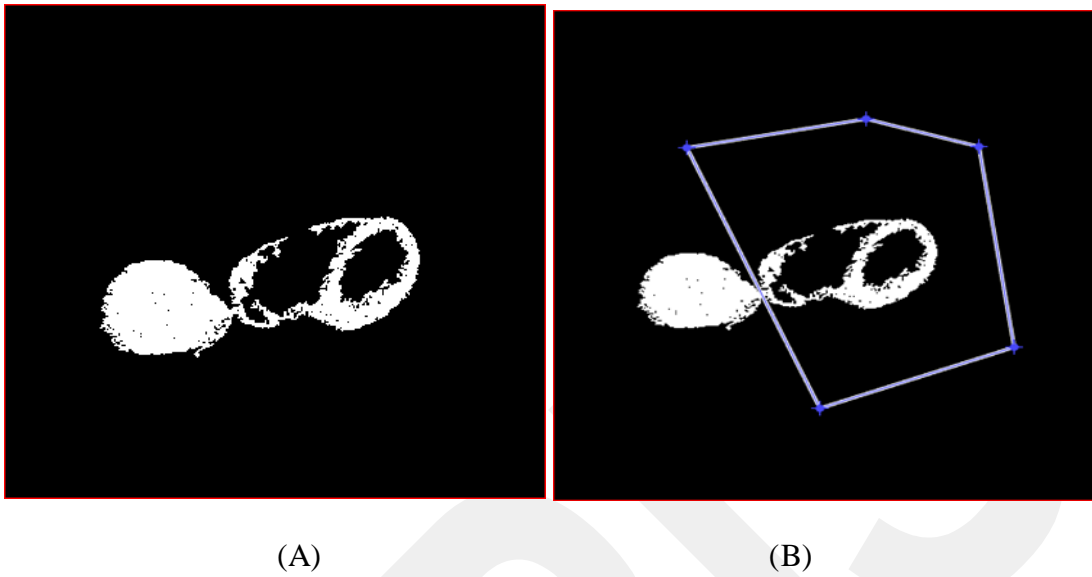
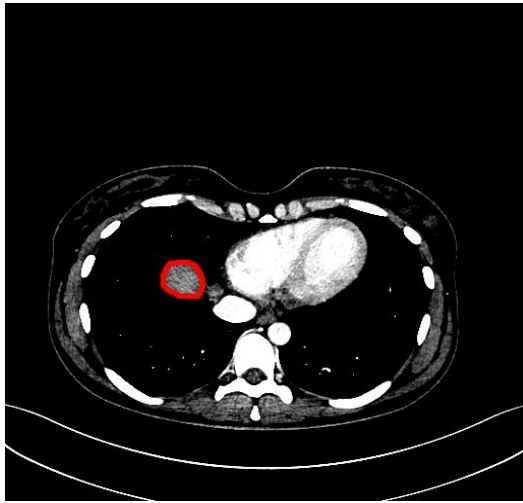


Figure 30 (A) Frame 56 Before Using Manually Operation, (B) Frame 56 After Using Manually Operation

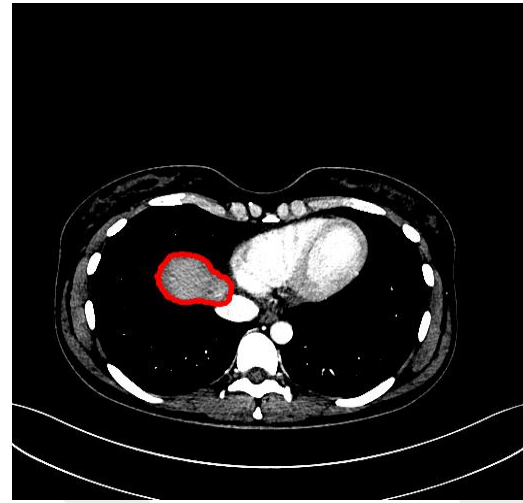


Figure 31 Frame 56 Segmented Image

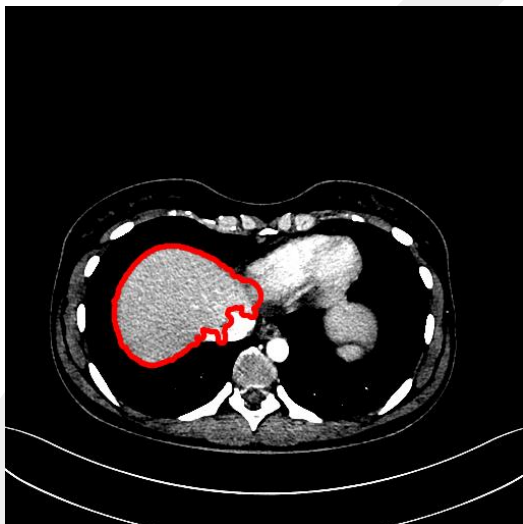
Liver shape is different from frame to another As shown :



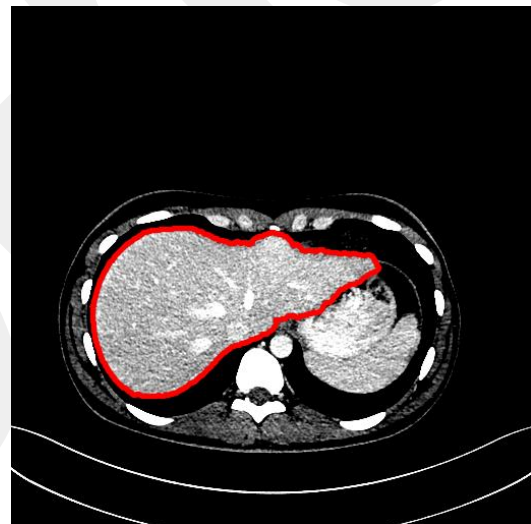
(A) Frame (50)



(B) Frame (52)



(C) Frame (66)

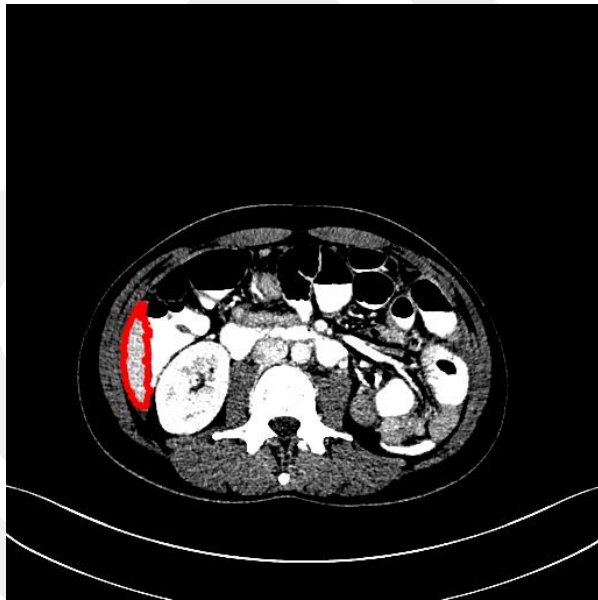


(D) Frame (81)



(E) Frame (101)

(F) Frame (200)



(G) Frame (295)

Figure 32 Different Shapes of Liver, (A) Frame (50), (B) Frame (52), (C) Frame (66), (D) Frame (81), (E) Frame (101), (F) Frame (200), (G) Frame (295)

Table-1 below shows the result of a simulation from Frame 50 to Frame 324

Frame Number	Area	Perimeter	Centroid (X)	Centroid (Y)
50	1013	121.854	175.3711747	284.7295163
51	1511	158.152	177.1291642	285.4260666
52	2267	219.054	181.2586677	287.071679
53	3121	236.108	180.2435117	286.8090356
54	3503	246.636	179.2206319	286.605455
55	4448	269.082	176.5809353	287.2823741
56	4714	300.616	176.1284326	287.2186312
57	5317	314.478	174.3041508	288.2552112
58	5619	325.99	173.2931005	288.5365316
59	6390	339.47	172.1514416	289.1182094
60	7349	349.914	171.3732481	289.7477208
61	7560	369.624	170.5291005	289.95
62	8117	441.268	172.3835161	289.8788961
63	8464	441.046	172.7646661	290.4393051
64	9370	459.528	172.236114	290.9750792
65	9520	475.614	170.7607863	291.6426411
66	10536	508.126	170.604309	291.8947418
67	10736	521.622	169.7705743	292.3568947
68	11401	526.088	170.2757521	292.7587277
69	11747	490.542	167.3787562	293.9006445
70	12365	563.09	171.3393752	293.4150405
71	13384	607.534	172.4785984	293.3490279
72	21280	893.592	222.6938959	291.7778276
73	22384	915.344	220.7394568	292.3847838
74	22561	896.462	219.8504038	291.9510613
75	22006	829.44	216.5648961	293.1670434

Frame Number	Area	Perimeter	Centroid (X)	Centroid (Y)
76	22282	858.742	216.2197854	292.7732731
77	22360	987.32	214.9298373	291.6226455
78	23483	985.46	214.1708821	291.1684753
79	23514	872.836	204.7374207	293.4627618
81	23657	881.542	210.923254	291.1797875
82	24751	941.114	210.1323814	290.2065402
83	24912	919.198	204.4259695	291.7375061
84	24870	881.6	205.5074406	290.1793923
85	25559	914.584	200.6757652	290.7712997
86	25601	901.962	199.3946695	289.8853195
87	25776	842.418	199.6694386	289.3692429
88	25880	886.526	195.8501932	289.9294436
89	25062	887.136	193.9385696	290.0579771
90	26189	808.37	191.8309559	290.5056488
91	26236	802.862	190.8007641	290.3912846
92	26529	785.824	190.6988748	290.6149504
93	26051	774.048	189.6428598	290.4149939
94	27398	774.294	189.36864	290.4129134
95	27501	783.608	188.4760191	290.5382713
96	27614	781.424	188.0983318	290.6121378
97	27062	787.412	187.4801511	290.7351935
98	27229	772.228	186.7949272	290.8903256
99	28410	793.418	186.013622	291.0428018
100	28583	776.388	185.5442396	291.0089564
101	28728	783.146	184.8353523	291.2160262
102	28777	776.678	184.5052283	291.3017566
103	28152	795.42	183.9955406	291.3867659
104	28234	789.788	183.2674625	291.6428132

Frame Number	Area	Perimeter	Centroid (X)	Centroid (Y)
105	28363	788.852	182.7879304	291.7054797
106	28408	815.286	182.3384506	291.784533
107	29504	789.67	181.5516879	291.9756304
108	29565	810.494	180.8943683	292.1511923
109	29668	806.014	180.6039504	292.1432857
110	29715	803.11	180.2103743	292.2152761
111	29755	829.856	180.0754799	292.3526957
112	29867	813.028	179.7555645	292.5567458
113	29068	821.768	179.3595517	292.4766862
114	29226	843.22	179.4186793	292.4627142
115	29276	851.748	179.3786828	292.3592945
116	29522	891.172	179.2610576	292.4973789
117	29620	880.048	178.8848465	292.2812541
118	30644	888.47	178.4251638	292.8432176
119	30651	865.188	178.6441628	292.7235672
120	30669	842.668	178.1160863	292.8610501
121	30678	827.368	177.7328673	292.8512538
122	30493	850.062	177.5774768	292.9781917
123	30474	825.208	177.5424544	292.8776411
124	30429	824.118	177.5899964	293.0235514
125	30419	832.734	177.1713547	292.9960379
126	30400	846.126	176.9836168	293.0093243
127	30398	826.764	176.8725097	292.9115984
128	30395	829.048	176.7492386	293.1518585
129	30381	841.418	176.4355901	293.0265632
130	30382	832.536	176.3171887	292.9007634
131	30378	870.942	176.711143	292.9307396
132	30373	860.804	176.6826951	292.9485849

Frame Number	Area	Perimeter	Centroid (X)	Centroid (Y)
133	30367	910.748	176.3912675	293.3401702
134	30309	916.436	175.8435448	292.8418951
135	30353	871.346	176.6149642	292.7553759
136	30345	848.868	175.9764339	292.7877732
137	30362	853.856	176.0344035	292.6512048
138	30359	849.928	175.9815818	292.7140747
139	30330	872.532	176.1304603	292.6182174
140	30294	902.932	175.2999934	292.4270716
141	30269	866.692	175.3465809	292.1377242
142	30232	846.032	175.2551932	292.5297367
143	30225	861.754	175.6694477	292.2088706
144	30209	864.104	175.4645635	292.0947731
145	29145	853.128	175.2706917	291.8618013
146	29127	890.958	175.9297663	291.6071581
147	29885	897.186	174.5757738	291.7843734
148	29735	910.184	173.7797881	291.9631411
149	29586	837.068	174.1624079	291.6382073
150	29510	817.59	174.1779058	291.6109116
151	29613	839.97	174.5512782	291.3252963
152	28521	876.21	173.89123	291.9008164
153	28280	825.034	173.9350068	291.385041
154	28454	899.02	173.223535	290.6506077
155	27252	872.986	173.3990838	291.5061534
156	27211	874.648	173.0772312	291.0120503
157	27762	855.038	172.8684723	290.5947431
158	26836	1099.716	168.1716984	290.5461759
159	25637	1119.97	167.541678	290.643484
160	25031	1079.222	168.4261457	290.7060044

Frame Number	Area	Perimeter	Centroid (X)	Centroid (Y)
161	25464	1094.448	167.9692145	291.0970505
162	25373	1035.53	167.6027733	290.5647957
163	24546	1067.222	165.3966838	291.0767131
164	23463	1071.794	166.8068341	290.4272323
165	22377	1049.432	166.5414181	290.7550947
166	20537	766.596	148.8566977	302.2445829
167	20634	768.444	149.4885141	302.4990792
168	20954	741.496	150.5685788	302.6420731
169	20862	723.814	149.9168824	302.4662544
170	20538	713.368	149.5078391	302.040559
171	20332	709.408	148.7915193	302.4259532
172	19317	753.936	148.6906531	302.5993503
173	19034	699.41	148.2040032	302.9064091
174	19026	686.11	149.919906	303.5883188
175	19761	736.114	147.7373109	302.7280502
176	19627	740.506	147.7531971	302.9716717
177	19557	738.924	148.7609861	303.0086185
178	19425	707.672	148.1699873	303.2417325
179	18222	694.116	147.429768	303.67095
180	18048	696.416	146.8195086	303.3218186
181	18423	672.414	146.5058798	303.5713365
182	18392	712.856	146.6463728	303.7929596
183	18203	687.878	146.9522002	303.1677806
184	18124	697.856	145.5985985	304.4771574
185	17805	709.908	145.4148003	304.7042725
186	17741	702.866	145.1258103	304.4706612
187	17602	688.938	145.3578692	304.880522
188	17352	661.59	144.7275818	305.1804403

Frame Number	Area	Perimeter	Centroid (X)	Centroid (Y)
189	16126	695.63	144.4332594	305.4510102
190	16739	672.356	143.9461963	305.3366589
191	16684	693.976	144.0622939	304.9180405
192	16506	673.078	143.4797061	305.4144887
193	16509	649.35	143.3805229	305.6083247
194	16353	663.98	142.8434135	305.9148465
195	15369	637.514	142.6739934	306.5771182
196	15390	624.994	142.2201402	306.8650096
197	15369	624.024	142.1050164	306.9059028
198	15282	622.686	141.8099727	306.4298531
199	14125	630.914	141.6453554	306.486876
200	14085	647.802	141.5447796	307.0560822
201	14679	618.84	141.2941058	306.0612944
202	14550	604.268	140.9852851	306.2985217
203	14345	615.366	140.9862069	306.5989075
204	14207	577.264	140.3696769	306.0620117
205	14152	607.858	140.1119276	305.9910967
206	13048	619.146	140.1019362	306.5315347
207	13655	621.744	139.8634898	306.1342888
208	13533	612.554	139.3456319	306.0060882
209	13381	578.77	138.8109259	305.6709513
210	13184	600.118	138.5878337	305.4280188
211	12876	574.058	138.2046085	305.6280055
212	12641	559.328	137.8310965	305.5977553
213	12527	563.074	137.4380139	305.4966073
214	12414	564.562	137.1581279	305.442001
215	12188	555.416	136.6782081	305.3274532
216	12002	560.09	136.3716881	305.2223796

Frame Number	Area	Perimeter	Centroid (X)	Centroid (Y)
217	11721	540.496	136.0677608	304.9339311
218	11616	528.71	136.0296334	304.8079822
219	11466	556.308	135.4985186	304.7302196
220	11254	563.736	135.3616079	304.0047813
221	11100	539.686	134.7769369	303.7361261
222	10210	531.308	134.579798	303.9561065
223	10203	542.53	134.3636787	303.6397654
224	10216	510.086	133.8443119	303.60212
225	10217	504.768	133.5092637	303.438322
226	10244	500.674	133.0587661	303.0000976
227	10005	485.82	132.7211394	302.8738631
228	9430	483.686	132.382706	302.9140387
229	9378	485.332	132.0671626	302.7603844
230	9178	481.428	131.7382359	302.6579447
231	9133	476.202	131.2273367	302.4075598
232	9102	490.848	131.034388	302.3651945
233	8725	461.968	130.6981575	302.2122836
234	8717	482.934	130.3887305	302.3929508
235	8522	444.378	129.7975912	302.0578812
236	8312	441.292	129.4057436	301.9598427
237	8238	450.63	129.2945023	301.7998305
238	8073	445.18	128.9264214	301.5063793
239	7745	441.434	128.6530197	301.7140496
240	7520	418.16	128.2703125	300.8014323
241	7247	436.164	128.1553385	300.8866306
242	7207	427.348	127.6495207	300.6345349
243	7139	414.926	127.2511397	300.3622047
244	7082	413.206	127.0251341	300.5488563

Frame Number	Area	Perimeter	Centroid (X)	Centroid (Y)
245	6521	401.768	126.5689929	300.2963445
246	6455	430.582	126.3927061	300.4654996
247	6400	429.252	125.9802985	300.749403
248	6312	420.444	125.6865373	301.0109365
249	6227	425.042	125.3552323	300.4486157
250	6116	386.038	124.7520207	299.9860976
251	6096	395.938	124.5625	300.1896325
252	5840	380.902	124.1887205	300.6686869
253	5775	376.52	123.7731602	300.6306494
254	5649	379.24	123.4060896	300.4661002
255	5551	393.45	123.2722032	300.5898036
256	5405	382.292	122.8564292	300.7652174
257	5270	366.66	122.600759	301.1155598
258	5143	364.122	122.3103247	301.3630177
259	5000	358.084	122.0344	301.0482
260	4741	348.078	121.8551526	300.7889777
261	4724	359.938	121.6332216	301.0578132
262	4638	348.002	121.390785	301.2440273
263	4523	353.106	121.2197251	301.4147938
264	4413	337.922	120.649898	301.8248357
265	4300	330.644	120.5216279	301.6509302
266	4227	322.092	120.3600662	301.6967116
267	4126	320.016	120.0896752	301.7615124
268	3769	317.246	119.7150416	302.6623835
269	3733	315.112	119.3313332	302.145317
270	3721	326.666	119.2842747	302.678865
271	3611	314.476	118.7806702	301.9160897
272	3525	309.786	118.9518881	302.6567832

Frame Number	Area	Perimeter	Centroid (X)	Centroid (Y)
273	3327	309.406	118.6681172	302.0565709
274	3318	307.528	118.149789	302.1163351
275	3244	305.104	117.9873613	302.0607275
276	3115	288.11	117.6378812	302.3573034
277	3018	279.78	117.4675282	302.4343936
278	2830	275.464	117.2829352	302.8505119
279	2711	264.01	117.0438008	303.8452844
280	2705	277.126	117.0032086	302.6616756
281	2628	274.836	116.5683346	303.06236
282	2614	268.468	116.3397093	303.2547819
283	2524	254.458	116.1764937	303.3580975
284	2435	258.428	115.9115152	303.8270707
285	2356	247.47	115.3382852	304.1668081
286	2225	236.098	115.0989107	303.9572985
287	2213	238.96	114.9538737	304.1885356
288	2150	239.34	114.7137615	303.5229358
289	2133	236.288	114.8895053	303.2020342
290	2116	235.594	114.7240076	303.7344045
291	1926	222.7	114.0647773	303.9023279
292	1914	228.456	114.3937438	303.7676266
293	1878	227.05	113.8988409	304.1643836
294	1854	223.412	113.7491909	304.2195254
295	1811	228.474	113.5963556	304.1314191
296	1743	214.612	113.4199656	304.2088353
297	1715	222.766	113.296793	304.0209913
298	1572	212.404	112.7142857	304.7661188
299	1561	202.322	112.7428752	304.8169728
300	1507	193.018	112.4200398	305.2501659

Frame Number	Area	Perimeter	Centroid (X)	Centroid (Y)
301	1426	191.34	112.1037868	305.016129
302	1405	193.614	112.0661922	305.1010676
303	1314	185.302	111.6788432	305.2838661
304	1268	184.674	111.3824921	305.2121451
305	1165	173.732	111.0861925	305.6242678
306	1114	171.152	110.572711	305.5933573
307	1063	162.84	110.3311383	305.2690499
308	989	154.81	109.9362993	305.0647118
309	929	155.364	109.8019376	306.4790097
310	870	146.382	109.3298851	306.2678161
311	827	147.574	109.1062574	305.2550177
312	726	134.638	108.7738095	305.8015873
313	646	126.286	108.1408669	305.4303406
314	601	118.76	107.8402662	305.6489185
315	552	115.874	107.5380435	305.8894928
316	502	110.068	107.1454183	305.5856574
317	443	107.298	107.2071882	305.4249471
318	336	102.146	106.8459596	307.4116162
319	305	88.202	105.9934426	307.747541
320	271	80.99	106.3780069	309.3333333
321	228	70.024	106.2982456	310.9649123
322	211	69.544	106.5194805	310.5108225
323	157	57.552	106.1468927	310.1412429
324	120	55.774	105.8	311.2666667

Table 1 Result of simulation from Frame 50 to Frame 324

After getting the value of the area from above table we calculate the volume by using according to this equation (4.6) .for this dataset we define a slice thickness of 1 mm. And pixel spacing 0.75×0.75 according to its header.

5.4 Accuracy

We have implemented quantitative enquiry in order to match the performance of the segmentation for the results that existed in chapter 5, which been gotten from multiple algorithms that we have shown in chapter 4. In the literature there are different performance measures in order to evaluate the algorithms and methods. In general, sensitivity, specificity and accuracy have been used Bhowmick et al (2013) [78], Biganzoli et al. (2013) [79] and Choi et al. (2013) [80].

There are definition for each measure, for instance, a TN (True Negative) is the number of pixels in the background that are categorized correctly, TP (True Positive) is the number of pixels in the foreground that are categorized correctly, a FP (False Positive) is the number of pixels in the background that are categorized as the foreground and a FN (False Negative) is the number of pixels in the foreground that are categorized as the background. The four possible characterizations are represented in Figure 32 as a confusion matrix. The exact characterization, which are the TP and TN, has been shown along the diagonal of the table. The errors model, which are the FP and FN, have been shown in another sections of the table.

		Observed	
		True	False
Predicted	True	True Positive (TP)	False Positive (FP)
	False	False Negative (FN)	True Negative (TN)

Figure 33 Confusion matrix

The sensitivity can be defined as the amount of facts that been recognized correctly through the diagnostic analysis. This is clear on the ability of the test in detecting disease. Moreover, specificity can be defined as the amount of the correct negatives that been recognized correctly through the diagnostic analysis. It suggests how good the test is at identifying a normal (negative) circumstance. Finally, the accuracy can be defined as the amount of true results as for, the true negative or the true positive in the population. It measures the degree of veracity of a diagnostic test on a condition.

$$\text{Sensitivity} = \frac{TP}{TP + FN} \quad (5.1)$$

$$\text{Specificity} = \frac{TN}{TN + FP} \quad (5.2)$$

$$\text{Accuracy} = \frac{TP + TN}{TP + TN + FP + FN} \quad (5.3)$$

Each segmentation technique that's been used in this study has been estimated through using three metrics. The values of the measures accuracy, sensitivity and specificity are shown in Table 2.

Frame Number	Accuracy	Specificity	Sensitivity
50	0.965775	0.999732	0.931818
51	0.998432	0.999301	0.997562
52	0.992351	0.999561	0.985141
53	0.976182	0.999699	0.952665
54	0.993433	0.999133	0.987733
55	0.984094	0.999488	0.968699
56	0.997078	0.999114	0.995042
57	0.998191	0.998983	0.997399
58	0.989698	0.999555	0.979841

Frame Number	Accuracy	Specificity	Sensitivity
59	0.984997	0.999397	0.970597
60	0.979797	0.999447	0.960147
61	0.992572	0.999156	0.985988
62	0.986286	0.998674	0.973898
63	0.989327	0.997694	0.98096
64	0.99338	0.9978	0.98896
65	0.99513	0.997776	0.992484
66	0.995937	0.998136	0.993739
67	0.992788	0.9981	0.987475
68	0.995549	0.997138	0.993959
69	0.993295	0.996268	0.990323
70	0.994152	0.996319	0.991984
71	0.995677	0.99441	0.996944
72	0.985121	0.981835	0.988408
73	0.979552	0.981137	0.977968
74	0.980649	0.97949	0.981807
75	0.987898	0.981292	0.994505
76	0.985443	0.980635	0.990252
77	0.986681	0.988547	0.984815
78	0.992975	0.989544	0.996407
79	0.992877	0.988773	0.996981
80	0.992095	0.987658	0.996532
81	0.993312	0.988821	0.997803
82	0.991697	0.989984	0.993411
83	0.994493	0.993599	0.995387
84	0.993539	0.990613	0.996466
85	0.988145	0.991612	0.984679
86	0.991676	0.992537	0.990816

Frame Number	Accuracy	Specificity	Sensitivity
87	0.989426	0.993902	0.984951
88	0.992907	0.994094	0.991721
89	0.990499	0.994853	0.986146
90	0.98471	0.997517	0.971903
91	0.99178	0.995978	0.987582
92	0.989483	0.996572	0.982394
93	0.990542	0.996349	0.984735
94	0.990869	0.997264	0.984475
95	0.991995	0.996665	0.987324
96	0.992583	0.996288	0.988879
97	0.99234	0.994987	0.989692
98	0.991856	0.99569	0.988021
99	0.994916	0.996017	0.993815
100	0.995317	0.995272	0.995363
101	0.995432	0.995019	0.995845
102	0.994856	0.994631	0.995082
103	0.993988	0.995795	0.992181
104	0.994127	0.995146	0.993108
105	0.989442	0.995488	0.983396
106	0.993903	0.995021	0.992785
107	0.990717	0.99559	0.985845
108	0.988999	0.9955	0.982497
109	0.979984	0.995397	0.96457
110	0.993116	0.993846	0.992386
111	0.995346	0.994481	0.996212
112	0.993658	0.993729	0.993586
113	0.993944	0.994186	0.993701
114	0.991629	0.993434	0.989824

Frame Number	Accuracy	Specificity	Sensitivity
115	0.989587	0.994341	0.984833
116	0.989948	0.993456	0.98644
117	0.987017	0.993121	0.980913
118	0.988615	0.992415	0.984815
119	0.988788	0.994742	0.982835
120	0.991371	0.993075	0.989666
121	0.994044	0.993506	0.994582
122	0.993878	0.993323	0.994433
123	0.994764	0.993471	0.996057
124	0.99394	0.994282	0.993599
125	0.993391	0.994082	0.9927
126	0.992163	0.993777	0.99055
127	0.99357	0.993823	0.993316
128	0.993889	0.992795	0.994984
129	0.993957	0.994066	0.993848
130	0.992156	0.994341	0.98997
131	0.992155	0.993669	0.990641
132	0.987728	0.993727	0.981728
133	0.991347	0.993476	0.989218
134	0.991811	0.993091	0.99053
135	0.990202	0.993449	0.986955
136	0.991448	0.992618	0.990279
137	0.99122	0.992965	0.989475
138	0.994046	0.992318	0.995773
139	0.992534	0.992158	0.99291
140	0.992918	0.992271	0.993565
141	0.99348	0.992205	0.994756
142	0.989069	0.992447	0.985691

Frame Number	Accuracy	Specificity	Sensitivity
143	0.993574	0.992522	0.994625
144	0.991079	0.98981	0.992347
145	0.99074	0.992776	0.988704
146	0.993646	0.992736	0.994556
147	0.990475	0.990484	0.990465
148	0.992141	0.992394	0.991888
149	0.99112	0.992635	0.989604
150	0.991207	0.992295	0.990119
151	0.989389	0.993322	0.985457
152	0.992723	0.993328	0.992118
153	0.991816	0.993673	0.989959
154	0.987381	0.992666	0.982096
155	0.992785	0.992932	0.992639
156	0.991148	0.992327	0.989969
157	0.99189	0.993264	0.990516
158	0.99306	0.993229	0.992891
159	0.993263	0.993355	0.993171
160	0.992063	0.993166	0.990959
161	0.990976	0.994702	0.98725
162	0.989602	0.995482	0.983723
163	0.984826	0.992613	0.977039
164	0.987249	0.992218	0.982279
165	0.962013	0.992585	0.931441
166	0.986599	0.991821	0.981378
167	0.98829	0.992264	0.984315
168	0.989362	0.991255	0.987468
169	0.983974	0.993492	0.974456
170	0.983406	0.992038	0.974774

Frame Number	Accuracy	Specificity	Sensitivity
171	0.986442	0.993196	0.979689
172	0.988195	0.992068	0.984322
173	0.98952	0.993603	0.985436
174	0.98853	0.996075	0.980985
175	0.991044	0.993821	0.988266
176	0.990161	0.996049	0.984273
177	0.990188	0.995435	0.984941
178	0.992645	0.996033	0.989256
179	0.992264	0.995821	0.988708
180	0.992993	0.995942	0.990044
181	0.992892	0.997066	0.988719
182	0.992748	0.995808	0.989687
183	0.989999	0.996638	0.983359
184	0.992134	0.997734	0.986535
185	0.993967	0.997581	0.990352
186	0.990823	0.99752	0.984126
187	0.994233	0.995808	0.992658
188	0.992153	0.996599	0.987708
189	0.993582	0.996696	0.990467
190	0.982342	0.997359	0.967325
191	0.994714	0.997208	0.99222
192	0.993918	0.997068	0.990768
193	0.992532	0.99685	0.988213
194	0.996634	0.996964	0.996304
195	0.99348	0.996513	0.990447
196	0.995252	0.997501	0.993003
197	0.995727	0.997551	0.993902
198	0.995007	0.997779	0.992234

Frame Number	Accuracy	Specificity	Sensitivity
199	0.991761	0.998132	0.98539
200	0.994418	0.997685	0.99115
201	0.996539	0.997675	0.995403
202	0.993281	0.997559	0.989003
203	0.995741	0.997541	0.993941
204	0.996725	0.997665	0.995784
205	0.99394	0.997489	0.990391
206	0.995532	0.997306	0.993758
207	0.994448	0.997423	0.991473
208	0.994365	0.997682	0.991047
209	0.994816	0.998149	0.991482
210	0.99493	0.998127	0.991734
211	0.994244	0.997792	0.990696
212	0.995574	0.997655	0.993493
213	0.993781	0.998275	0.989286
214	0.99584	0.997917	0.993764
215	0.992793	0.998138	0.987448
216	0.993276	0.997506	0.989046
217	0.993923	0.998133	0.989713
218	0.992096	0.997915	0.986277
219	0.993519	0.997663	0.989376
220	0.993499	0.998141	0.988857
221	0.993249	0.998051	0.988448
222	0.992173	0.998342	0.986003
223	0.992575	0.998165	0.986985
224	0.994993	0.998301	0.991685
225	0.988773	0.998634	0.978912
226	0.993388	0.998034	0.988741

Frame Number	Accuracy	Specificity	Sensitivity
227	0.987642	0.99845	0.976834
228	0.992108	0.998428	0.985787
229	0.998442	0.998288	0.998596
230	0.995087	0.998289	0.991885
231	0.993037	0.998475	0.987599
232	0.994356	0.998394	0.990319
233	0.998675	0.998289	0.999062
234	0.995765	0.998345	0.993185
235	0.99741	0.99837	0.996449
236	0.996313	0.998465	0.994161
237	0.995099	0.998407	0.991791
238	0.996731	0.998506	0.994956
239	0.995558	0.998323	0.992792
240	0.997142	0.998748	0.995537
241	0.99698	0.998404	0.995557
242	0.99548	0.998788	0.992172
243	0.995926	0.998629	0.993224
244	0.996407	0.998704	0.99411
245	0.995812	0.998705	0.992918
246	0.996759	0.998576	0.994942
247	0.993019	0.99853	0.987508
248	0.993919	0.998519	0.989319
249	0.994538	0.998481	0.990596
250	0.996605	0.998658	0.994552
251	0.997558	0.998592	0.996525
252	0.994847	0.99883	0.990864
253	0.995887	0.998843	0.992931
254	0.984806	0.998531	0.971081

Frame Number	Accuracy	Specificity	Sensitivity
255	0.993041	0.998739	0.987344
256	0.994682	0.998728	0.990636
257	0.993212	0.998779	0.987644
258	0.991862	0.998911	0.984812
259	0.993206	0.998943	0.987469
260	0.994034	0.998986	0.989082
261	0.986528	0.998975	0.974082
262	0.996162	0.998875	0.993449
263	0.997217	0.998848	0.995587
264	0.992564	0.999069	0.986059
265	0.993706	0.999085	0.988327
266	0.989674	0.999047	0.9803
267	0.998226	0.998804	0.997648
268	0.994636	0.999087	0.990186
269	0.990537	0.999207	0.981867
270	0.989911	0.999037	0.980785
272	0.989389	0.998926	0.979852
273	0.987982	0.999227	0.976737
274	0.987124	0.999239	0.975008
275	0.986279	0.99922	0.973338
276	0.987458	0.999371	0.975545
277	0.992055	0.999198	0.984912
278	0.991699	0.999237	0.984161
279	0.98505	0.999248	0.970853
280	0.982144	0.999233	0.965056
281	0.990903	0.999102	0.982704
282	0.98959	0.99918	0.98
283	0.992708	0.999092	0.986325

Frame Number	Accuracy	Specificity	Sensitivity
284	0.991244	0.999269	0.983219
285	0.988225	0.999438	0.977011
286	0.978731	0.999427	0.958036
287	0.977283	0.999504	0.955061
288	0.985928	0.999366	0.97249
289	0.988047	0.999293	0.976802
290	0.986016	0.99917	0.972862
291	0.977674	0.999481	0.955867
292	0.982455	0.999301	0.965608
293	0.980652	0.999451	0.961853
294	0.981661	0.999439	0.963883
295	0.987028	0.99904	0.975016
296	0.988794	0.999202	0.978385
297	0.99068	0.999206	0.982155
298	0.990368	0.999382	0.981354
299	0.99429	0.999325	0.989255
300	0.987119	0.999417	0.97482
301	0.986771	0.999436	0.974105
302	0.995946	0.999276	0.992617
303	0.995866	0.999418	0.992314
304	0.990867	0.999402	0.982332
305	0.993086	0.999418	0.986755
306	0.991924	0.999376	0.984472
307	0.996432	0.999414	0.99345
308	0.981969	0.999533	0.964405
309	0.99017	0.999399	0.98094
310	0.986768	0.999476	0.97406
311	0.999665	0.999331	1

Frame Number	Accuracy	Specificity	Sensitivity
312	0.959779	0.999614	0.919944
313	0.937336	0.999671	0.875
314	0.99884	0.999645	0.998035
315	0.994148	0.999583	0.988713
316	0.959735	0.999648	0.919822
317	0.971083	0.999522	0.942643
318	0.988727	0.999675	0.977778
319	0.944067	0.999687	0.888446
320	0.991523	0.999782	0.983264
321	0.966281	0.99987	0.932692
322	0.972458	0.999794	0.945122
323	0.961225	0.99987	0.922581
324	0.961458	0.99984	0.923077

Table 2 Assessment of accuracy and specificity and sensitivity from frame 50 to

324

CHAPTER 6

CONCLUSION AND FUTURE WORK

6.1 Conclusion

In our study, proposed algorithms aim to compute liver volume from computed tomography (CT). We have introduced the two most important approaches that are used steady to segment and merge the images which are edge detection and region growing. Firstly, the segmentation based on edge region growing which combining the edge based segmentation advantage with the region growing segmentation and the definition of edge based image and the edge region image the border that detected will be accurate. Furthermore, after segmenting the whole slices, the live volume has been calculated. Finally, the algorithm that we have proposed and implemented on the data set is considered very successful on the image of CT type because the object that showing an area for a set of pixels will be easy to choice objects in the foreground in order to split them from the noise and from the background.

6.2 Future Work

The future work of potential area will be expanded the proposed method to use it for:

- Finding the volume of other organs in the body.
- Developing segmentation algorithms in order to be able to find the diagnosis of tumors in various organs of the body.

REFERENCES

1. **Zhang, Y.J. ed., (2006)**, “*Advances in image and video segmentation*”. IGI Global.
2. **Tsai, D., (1994)**, “*Automatic segmentation of liver structure in CT images using a neural network*”. IEICE Trans. Fundamentals E77-A, 11, 1892–1895.
3. **Husain, S.A. and Shigeru, E., (2000)**, “*Use of neural networks for feature based recognition of liver region on CT images*”. In Neural Networks for Signal Processing X, 2000. Proceedings of the 2000 IEEE Signal Processing Society Workshop (Vol. 2, pp. 831-840). IEEE.
4. **Lee, C.C., Chung, P.C. and Tsai, H.M., (2003)**, “*Identifying multiple abdominal organs from CT image series using a multimodule contextual neural network and spatial fuzzy rules*”. Information Technology in Biomedicine, IEEE Transactions on, 7(3), pp.208-217.
5. **Bae, K.T., Giger, M.L., Chen, C.T. and Kahn Jr, C.E., (1993)**, “*Automatic segmentation of liver structure in CT images*”. Medical physics, 20(1), pp.71-78.
6. **Gao, L., Heath, D.G., Kuszyk, B.S. and Fishman, E.K., (1996)**, “*Automatic liver segmentation technique for three-dimensional visualization of CT data*”. Radiology, 201(2), pp.359-364.
7. **Barrett, W.A. and Mortensen, E.N., (1997)**, “*Interactive live-wire boundary extraction*”. Medical image analysis, 1(4), pp.331-341.
8. **Schenk, A., Prause, G.P. and Peitgen, H.O., (2001)**, “*July. Local-cost computation for efficient segmentation of 3D objects with live wire*”. In Medical Imaging 2001 (pp. 1357-1364). International Society for Optics and Photonics.
9. **Beichel¹², R., Bauer, C., Bornik, A., Sorantin, E. and Bischof, H., (2007)**, “*Liver segmentation in CT data: A segmentation refinement approach*”. Proceedings of" 3D Segmentation in The Clinic: A Grand Challenge, pp.235-245.

10. **Boykov, Y. and Funka-Lea, G., (2006),** “*Graph cuts and efficient ND image segmentation*”. International journal of computer vision, 70(2), pp.109-131.
11. **Beck, A. and Aurich, V., (2007),** “*HepaTux-a semiautomatic liver segmentation system*”. 3D Segmentation in The Clinic: A Grand Challenge, pp.225-233.
12. **Dawant, B.M., Li, R., Lennon, B. and Li, S., (2007),** “*Semi-automatic segmentation of the liver and its evaluation on the MICCAI 2007 grand challenge data set*”. 3D Segmentation in The Clinic: A Grand Challenge, pp.215-221.
13. **Pan, S. and Dawant, B.M., (2001),** “*Automatic 3D segmentation of the liver from abdominal CT images: a level-set approach*”. In Medical Imaging 2001 (pp. 128-138). International Society for Optics and Photonics.
14. **Slagmolen P, Elen A, Seghers D, Loeckx D, Maes F, Haustermans, K (2007),** “*Atlas based liver segmentation using nonrigid registration with a B-spline transformation model*”. In: Proceedings of MICCAI workshop on 3D segmentation in the clinic: a grand challenge, pp 197-206.
15. **Wimmer, A., Soza, G. and Hornegger, J., (2007),** “*Two-stage semi-automatic organ segmentation framework using radial basis functions and level sets*”. 3D Segmentation in The Clinic: A Grand Challenge, pp.179-188.
16. **McInerney, T., Terzopoulos, D.,(2000).** “*T-snakes: Topologically Adaptive Snakes*”. Med. Image Anal. 4(2),73–91.
17. **Maes, F., Collignon, A., Vandermeulen, D., Marchal, G. and Suetens, P., (1997),** “*Multimodality image registration by maximization of mutual information*”. Medical Imaging, IEEE Transactions on, 16(2), pp.187-198.
18. **Rueckert, D., Sonoda, L.I., Hayes, C., Hill, D.L., Leach, M.O. and Hawkes, D.J., (1999),** “*Nonrigid registration using free-form deformations: application to breast MR images*”. Medical Imaging, IEEE Transactions on, 18(8), pp.712-721.
19. **Gao, L., Heath, D.G. and Fishman, E.K., (1998),** “*Abdominal image segmentation using three-dimensional deformable models*”. Investigative Radiology, 33(6), pp.348-355.
20. **Montagnat, J. and Delingette, H., (1997),** “*Volumetric medical images segmentation using shape constrained deformable models*”. In CVRMed-MRCAS'97 (pp. 13-22). Springer Berlin Heidelberg.

21. Soler L, Delingette H, Malandain G, Montagnat J, Ayache N, Koehl C, Dourthe O, Malassagne B, Smith M, Mutter D, Marescaux J (2001), “Fully automatic anatomical, pathological, and functional segmentation from ct scans for hepatic surgery”. *Comput Aided Surg* 6(3):131-142.
22. Lamecker, H., Lange, T. and Seebass, M., (2004), “Segmentation of the liver using a 3D statistical shape model (pp. 04-09)”. Konrad-Zuse-Zentrum für Informationstechnik.
23. McLachlan GJ, Krishnan T (2009), “*The EM algorithm and extensions*”, 2nd edn. Wiley-Interscience, Hoboken.
24. Weickert, J., Romeny, B.T.H. and Viergever, M.A., (1998), “Efficient and reliable schemes for nonlinear diffusion filtering. *Image Processing*”, IEEE Transactions on, 7(3), pp.398-410.
25. Sonka M, Hlavac V, Boyle R (2007), “*Mathematical morphology in image processing, analysis, and machine vision*”. Thomson, New York.
26. Saddi, K.A., Rousson, M., Chafd’hotel, C. and Cheriet, F., (2007), “October. *Global-to-local shape matching for liver segmentation in CT imaging*”. In Proceedings of MICCAI workshop on 3D segmentation in the clinic: a grand challenge (pp. 207-214).
27. Tsai, A., Yezzi Jr, A., Wells, W., Tempany, C., Tucker, D., Fan, A., Grimson, W.E. and Willsky, A., (2003), “A shape-based approach to the segmentation of medical imagery using level sets”. *Medical Imaging, IEEE Transactions on*, 22(2), pp.137-154.
28. Rousson M, Cremers D (2005), “Efficient kernel density estimation of shape and intensity priors for level set segmentation”. In: Proceedings of MICCAI, pp 757-764.
29. Rikxoort E, Arzhaeva Y, Ginneken B (2007), “Automatic segmentation of the liver in computed tomography scans with voxel classification and atlas matching”. In: Proceedings of MICCAI workshop on 3D segmentation in the clinic: a grand challenge, pp 101-108.
30. Zhang, Y, J (2001), “An overview of image and video segmentation in the last 40 years” Proceedings of the 6th International Symposium on Signal Processing and Its Applications, pp. 148-151.

- 31. Rusko, L., Bekes, G., Nemeth, G. and Fidrich, M., (2007),** “*Fully automatic liver segmentation for contrast-enhanced CT images. MICCAI Wshp*”. 3D Segmentation in the Clinic: A Grand Challenge, 2(7).
- 32. Cover, T.M. and Hart, P.E., (1967),** “*Nearest neighbor pattern classification*”. Information Theory, IEEE Transactions on, 13(1), pp.21-27.
- 33. Mattes D, Haynor DR, Vesselle H, Lewellen TK, Eubank W (2003),** “*PET-CT image registration in the chest using free-form deformations*”. IEEE Trans Med Imaging 22(1):120-128.
- 34. Rohlfing T, Brandt R, Menzel R, Russakoff DB, Maurer CR (2005),** “*Quo vadis, atlas-based segmentation? Handbook of medical image analysis—Volume III: Registration models*”. Kluwer Academic, Norwell MA, pp 435-486.
- 35. Sonka M, Hlavac V, Boyle R (2007),** “*Mathematical morphology in image processing, analysis, and machine vision*”. Thomson, Newyork.
- 36. Suganya, R., & Rajaram, S. (2012),** “*Classification of liver diseases from ultrasound images using a hybrid kohonen SOM and LPND speckle reduction method*”. In Signal Processing, Computing and Control (ISPC), International Conference on (pp. 1-6). IEEE.
- 37. Lu J., Wang D., Shi L., & Heng P. A., (2012),** “*Automatic liver segmentation in CT images based on support vector machine*”. In Biomedical and Health Informatics (BHI), IEEE-EMBS International Conference on (pp. 333-336).
- 38. Mortelé, K.J., Cantisani, V., Troisi, R., de Hemptinne, B. and Silverman, S.G., (2003),** “*Preoperative liver donor evaluation: imaging and pitfalls*”. Liver Transplantation, 9(9).
- 39. Bogetti, J., Herts, B.R., Sands, M.J., Carroll, J.F., Vogt, D.P. and Henderson, J.M., (2001),** “*Accuracy and utility of 3-dimensional computed tomography in evaluating donors for adult living related liver transplants*”. Liver Transplantation, 7(8), pp.687-692.
- 40. Tsai, D., (1994).** “*Automatic segmentation of liver structure in CT images using a neural network*”. IEICE Trans. Fundamentals E77-A, 11, 1892–1895.
- 41. Nowozin, S., Lixu, G., (2005),** “*A novel Liver Perfusion Analysis Method*”, *IEEE Engineering in Medicine and Biology 27th Annual Conf*”, Shanghai, China, September 1-4, 3063-3066.

- 42. Hermoye, L., Laamari-Azjal, I., Cao, Z., Annet, L., Lerut, J., Dawant, B. M., Van Beers, B. E., (2005),** “*Liver segmentation in living liver transplant donors: Comparison of semiautomatic and manual methods*”. International Journal of Radiology, 234, 171-178.
- 43. Strzelecki, M., de Certaines, J. and Ko, S., (2007),** “*November. Segmentation of 3D MR liver images using synchronised oscillators network*”. In Information Technology Convergence, 2007. ISITC 2007. International Symposium on (pp. 259-263). IEEE.
- 44. Kumar, S.S., Moni, R.S. and Rajeesh, J., (2013),** “*An automatic computer-aided diagnosis system for liver tumours on computed tomography images*”. Computers & Electrical Engineering, 39(5), pp.1516-1526.
- 45. Xiaoqi Lu, Jianshuai Wu, Xiaoying Ren, Baohua Zhang and Yinhui Li,(2014),** “*The study and application of the region growing algorithm for liver segmentation*”, OPTIK 125, pp.2142-2147.
- 46. Sangewar, S., Peshattiwar, A.A., Alagdeve, V. and Balpande, R., (2013),** September. “*Liver segmentation of CT scan images using K means algorithm*”. In Advanced Electronic Systems (ICAES), 2013 International Conference on (pp. 6-9). IEEE.
- 47. Suhuai Luo, Jesse.S.Lin, Stephen K.Chalup and Guoyu Kian,(2009),** “*A liver segmentation algorithm based on wavelets and machine learning*”, IEEE International Conference on Computational Intelligence and Natural Computing, pp.122-125.
- 48. Hans Bhurkhardt and Wan Nural Jawahir WanYussof,(2009),** “*3D volumetric CT liver segmentation using hybrid segmentation techniques*”, IEEE International Conference on Soft Computing and Pattern Recognition, pp.404-40S.
- 49. Song, X., Cheng, M., Wang, B., Huang, S. and Huang, X., (2013),** July. “*Automatic liver segmentation from CT images using adaptive fast marching method*”. In Image and Graphics (ICIG), 2013 Seventh International Conference on (pp. 897-900). IEEE.
- 50. Yi, X., Zhong, L. and Lin, J., (2010),** October. “*Liver ct image segmentation by local entropy method*”. In Computer Application and System Modeling (ICCAS), 2010 International Conference on (Vol. 11, pp. V11-591). IEEE.

- 51. Huang, Y., Wang, J., Sun, J. and Huang, L., (2013),** October. “*Liver segmentation in CT images based on region-scalable fitting model*”. In Anti-Counterfeiting, Security and Identification (ASID), 2013 IEEE International Conference on (pp. 1-4). IEEE.
- 52. Hwang, K.H. and Jung, J.W., (2009),** August. “*Segmentation of the liver in CT images using pseudocolorization and labeling methods*”. In Fuzzy Systems, 2009. FUZZ-IEEE 2009. IEEE International Conference on (pp. 2170-2174). IEEE.
- 53. Abdel-massieh, N.H., Hadhoud, M.M. and Moustafa, K.A., (2010),** March. “*A fully automatic and efficient technique for liver segmentation from abdominal CT images*”. In Informatics and Systems (INFOS), 2010 The 7th International Conference on (pp. 1-8). IEEE.
- 54. Elmasry, W.H., El-Bendary, N. and Hassanien, A.E., (2012),** September. “*Graph Partitioning based Automatic Segmentation Approach for CT Scan Liver Images*”. In FedCSIS (pp. 183-186).
- 55. Mancas, M., Gosselin, B. and Macq, B., (2005),** March. “*Segmentation using a region-growing thresholding*”. In Electronic Imaging 2005 (pp. 388-398). International Society for Optics and Photonics.
- 56. Pohle, R. and Toennies, K.D., (2001),** September. “*A new approach for model-based adaptive region growing in medical image analysis*”. In Computer Analysis of Images and Patterns (pp. 238-246). Springer Berlin Heidelberg.
- 57. Liu, L. and Sclaroff, S., (2004).** “*Deformable model-guided region split and merge of image regions*”. Image and Vision Computing, 22(4), pp.343-354.
- 58. Carr, J.C., Beatson, R.K., Cherrie, J.B., Mitchell, T.J., Fright, W.R., McCallum, B.C. and Evans, T.R., (2001),** “*August. Reconstruction and representation of 3D objects with radial basis functions*”. In Proceedings of the 28th annual conference on Computer graphics and interactive techniques (pp. 67-76). ACM.
- 59. Cootes TF, Hill A, Taylor CJ, Haslam J (1994),** “*Use of active shape models for locating structures in medical images*”. Imag Vis Comput 12(6):355-366.
- 60. Kainmüller D, Lange T, Lamecker H (2007),** “*Shape constrained automatic segmentation of the liver based on a heuristic intensity model*”. In: Proceedings of MICCAI workshop on 3D segmentation in the clinic: a grand challenge, pp 109-116

- 61. McLachlan, G.J. and Krishnan, T., (1998),** *“The EM Algorithm and Extensions”*. Statistics in Medicine, 17, pp.1187-1187.
- 62. Sonka M, Hlavac V, Boyle R (2007),** Mathematical morphology in image processing, analysis, and machine vision. Thomson, Newyork.
- 63. Susomboon R, Raicu DS, Furst J (2007),** *“Ahybrid approach for liver segmentation”*. In: Proceedings of MICCAI workshop on 3D segmentation in the clinic: a grand challenge, pp 151-160.
- 64. Haralick RM, Shanmugam K, Dinstein I (1973),** *“Textural features for image classification”*. IEEE Trans Syst Man Cybern 3(6):610-621.
- 65. Duda RO, Hart PE, Stork DG (2000),** *“Pattern classification”*. 2nd edn. Wiley interscience, New York.
- 66. Chi, Y., Cashman, P.M., Bello, F. and Kitney, R.I., (2007), October.** *“A discussion on the evaluation of a new automatic liver volume segmentation method for specified CT image datasets”*. In Proceedings of 10th International Conference on Medical Image Computing and Computer Assisted Intervention (pp. 167-168).
- 67. Tsai D, Tanahashi N (1994),** *“Neural-network-based boundary detection of liver structure in ct images for 3-d visualization”*. In: Proceedings of IEEE international conference neural networks, pp 3484-3489.
- 68. Koss JE, Newman FD, Johnson TK, Kirch DL (1999),** *“Abdominal organ segmentation using texture transforms and a hopfield neural network”*. IEEE Trans Med Imaging 18(7):640-648.
- 69. Yang, Y., Huang, S., Lin, P. and Rao, N., (2008), October.** *“Medical image segmentation based on level set combining with region information”*. In Natural Computation, 2008. ICNC'08. Fourth International Conference on (Vol. 5, pp. 70-74). IEEE.
- 70. Chen, Y.T. and Tseng, D.C.,(2008).** *“Medical image segmentation based on the Bayesian level set method”*. In Medical Imaging and Informatics (pp. 25-34). Springer Berlin Heidelberg.
- 71. Cremers, D., Rousson, M. and Deriche, R., (2007).** *“A review of statistical approaches to level set segmentation: integrating color, texture, motion and shape”*. International journal of computer vision, 72(2), pp.195-215.

- 72. Brejl, M. and Sonka, M., (1998), May.** “*Edge-based image segmentation: machine learning from examples*”. In Neural Networks Proceedings, 1998. IEEE World Congress on Computational Intelligence. The 1998 IEEE International Joint Conference on (Vol. 2, pp. 814-819). IEEE.
- 73. Godbole, S. and Amin, A., (1995),** “*Mathematical morphology for edge and overlap detection for medical images*”. Real-Time Imaging, 1(3), pp.191-201.
- 74. Ting, L., Xiaogang, L., Chenglin, P. and Li, W., (2007), July.** “*Improved Morphological Edge Detection Algorithm for Ultrasound Heart Ventricular Wall Image in the Motion of Its Rotation*”. In Bioinformatics and Biomedical Engineering, 2007. ICBBE 2007. The 1st International Conference on (pp. 960-963). IEEE.
- 75. S.H Kim, D.O Kim, J.S. Kang ET. Al (2001),** “*Detection of Edges*”, Proc. Spie Capturer Analysis, and Display of Image Sequences III”, Vol. 4308, San Jose, A.
- 76. R. C.Gonzales, R. E. Woods,(2002) ,** “*Digital Image Processing*”, ISBN: 0-201-18075-8, 2nd Edition, Prentice Hall, 2002.
- 77. Stewart, R.D., Fermin, I. and Opper, M., (2002),** “*Region growing with pulse-coupled neural networks: an alternative to seeded region growing*”. Neural Networks, IEEE Transactions on, 13(6), pp.1557-1562.
- 78. Chen, W., Zhuang, H., Cheng, G., Torigian, D.A. and Alavi, A., (2013),** “*Comparison of FDG-PET, MRI and CT for post radiofrequency ablation evaluation of hepatic tumors*”. Annals of nuclear medicine, 27(1), pp.58-64.
- 79. Bhowmick, T., Mirrett, S., Reller, L. B., Price, C., Qi, C., Weinstein, M. P., Kirn, T. J., (2013),** “*Controlled Multicenter Evaluation of a Bacteriophage Based Method for the Rapid Detection of Staphylococcus aureus in Positive Blood Cultures*”. Journal of Clinical Microbiology (JCM.02967-12), 51(4), 1226-30.
- 80. Choi, J.H., Park, K. and Kim, Y.D., (2013),** “*Comparison of clinical utility between new and old bleeding criteria: a prospective study of evaluation for the bleeding academic research consortium definition of bleeding in patients with undergoing percutaneous intervention*”. Journal of the American College of Cardiology,61(10_S).

APPENDICES A

CURRICULUM VITAE

PERSONAL INFORMATION

PERSONAL INFORMATION

Surname, Name: SALIHI, Sara

Date and Place of Birth: 09 December 1988, Kirkuk

Marital Status: Single

Phone: +90 5386098955

Email: sara88esam@gmail.com



EDUCATION

Degree	Institution	Year of Graduation
M.Sc.	Çankaya Univ., Computer Engineering	2013-2015
B.Sc.	Cihan University	2008-2012
High School	Kirkuk lisesi	2006

FOREIN LANGUAGES

Arabic, English, Turkish, Kurdish, Türkmençe

HOBBIES

Swimming, Computer, Volleyball, Music, Shopping.